A Matrix Isolation Infrared and Ab-Initio Study of the Phenylacetylene-Acetylene Heterodimer

Kapil Dave

A dissertation submitted for the partial fulfilment of BS-MS dual degree in Science

Indian Institute of Science Education and Research, Mohali
April 2013

Certificate of Examination

This is to certify that the dissertation titled "A Matrix Isolation Infrared and Ab-Initio Study of the Phenylacetylene-Acetylene Heterodimer" submitted by Mr. Kapil Dave (Reg.No. ms08027) for the partial fulfilment of BS-MS dual degree programme of the Institute, has been examined by the thesis committee duly appointed by the Institute. The committee finds the work done by the candidate satisfactory and recommends that the report be accepted.

Dr. Ramesh Ramachandran **Dr. K.R Shamsundar** **Prof. K.S Viswanathan (Supervisor)**

Dated: April 26th, 2013

Declaration

The work presented in this dissertation has been carried out by me under the guidance of Prof. K.S Viswanathan at the Indian Institute of Science Education and Research Mohali (IISER-M).

This work has not been submitted in part or in full for a degree, a diploma, or a fellowship to any other university or institute. Whenever contributions of others are involved, every effort is made to indicate this clearly, with due acknowledgement of collaborative research and discussions. This thesis is a bonafide record of original work done by me and all sources listed within have been detailed in the bibliography.

Kapil Dave

Dated: April 13th, 2012

In my capacity as the supervisor of the candidate's project work, I certify that the above statements by the candidate are true to the best of my knowledge.

Prof. K.S Viswanathan

(Supervisor)

Certificate of Examination

This is to certify that the dissertation titled "A Matrix Isolation Infrared and Ab-Initio Study of the Phenylacetylene-Acetylene Heterodimer" submitted by Mr. Kapil Dave (Reg.No. ms08027) for the partial fulfilment of BS-MS dual degree programme of the Institute, has been examined by the thesis committee duly appointed by the Institute. The committee finds the work done by the candidate satisfactory and recommends that the report be accepted.

Dr. Ramesh Ramachandran **Dr. K.R Shamsundar** **Prof. K.S Viswanathan**

(Supervisor)

Dated: April 13th, 2013

Poster Presented

Best Poster Prize for presenting poster titled **“Understanding the Weak Non-Covalent interaction in Phenylacetylene-Acetylene Heterodimer”** in **MCBR3** (Modelling Chemical and Biological Re (activity)-3) Indo-German conference.

Acknowledgements

I would like to express my sincere gratitude to my master dissertation supervisor Prof. K. S Viswanathan, Head of the Department of Chemical Sciences, IISER-Mohali. It was a good opportunity to gain experience and learn the intricacies involved in building a scientific instrument. His valuable discussions and suggestions during the past one year period regarding setting up the instrument, computational calculations as well as in data analysis, made it comfortable for me to complete my thesis. His dedication and involvement right from the beginning (an empty room) to a fully functional Matrix isolation lab have inspired me towards science. I have enjoyed the work under his guidance. I have learnt an important aspect of life from him which is being independent and self sufficient. He himself screwed many nuts and lifted numerous cartoons during the course of establishing our facility. It was a nice time working with my lab members Mr. Bishnu Prasad Kar, Mr. Gaurav Kumar and Ms. Ginny Karir and I would like to thank them for equally contributing in setting up the laboratory. I owe my sincere thanks to the master thesis committee members, Dr.Ramesh Ramachandran and Dr K.R Shamsundar for spending their valuable time in evaluating my work at every step. I would like to thank Prof. N. Sathyamurthy Director, IISER-Mohali for supporting and motivating me at all times. I am grateful for the financial support provided by the Department of Science and Technology (DST) INSPIRE fellowship during my stay at IISER- Mohali. I heartily thank computing facility at IISER- Mohali especially scientific officer Dr. Paramdeep Singh Chandi for rendering me excellent computational facilities to carry out my theoretical research.I wish to thank my friends Mehreen Khaleel and D.J Pradeep for providing me with their joyful company, for understanding and believing in me. Last but not the least I would like to express my appreciation to my mother Mrs. Sarla Dave for being my constant support during my tough times, my father Mr. Puran Prakash Dave and sister Mrs. Ronak Dave for their encouragement and blessings.

CONTENTS

List of Figures

List of tables

List of Abbreviations

Abbreviation	Full form
AC	Acetylene
AIM	Atoms-in-Molecules
B3LYP	Becke-3-Parameter-Lee-Yang-Parr functional
BCP	Bond Critical Point
BLYP	Becke-Lee-Yang-Parr functional
BSSE	Basis Set Superposition Error
CCSD	Coupled-Cluster methods
CP	Critical Point
F.C.C	Face centre cubic
FTIR	Fourier Transform Infrared
H.C.P	Hexagonal close packing
HF	Hartree-Fock
IUPAC	International Union of Pure and Applied Chemistry
MP2	Møller-Plesset second order perturbation
M I	Matrix Isolation
M05	Minnesota type DFT functional
M06	Minnesota type DFT functional
PA	Phenylacetylene
ZPE	Zero point energy

Abstract

In this work, a study of weak non-covalent interactions such as C-H---π and π stacking interactions, has been done computationally, employing phenylacetylene and acetylene heterodimer as the system. The experimental facility to study these interactions has also been set up. The prime motivation behind choosing this as a system is that phenylacetylene and acetylene are molecules with multifunctional sites for hydrogen bonding. Therefore it becomes interesting to investigate the hierarchy of hydrogen bonding in such systems. The molecular structure, stabilization energies and vibrational frequencies were computed at MP2(full), M05-2X, M06-2X, and B3LYP levels of theory using 6-311++G(d,p) basis set. Computational studies resulted into four possible types of complexes, with the number and type of the complexes depending mainly on the applied level of theory. In addition to three geometries which involved C-H---π interactions, a π stacked complex was also obtained. The interaction energy of all the four complexes varied with the level of theory employed in the computation. Matrix isolation infrared spectroscopy, an experimental technique well suited for potentially studying such systems was set up at IISER-Mohali. This technique will be used to investigate the 1:1 adduct of phenylacetylene and acetylene in Ar or N_2 matrix. The adduct will be generated by depositing acetylene and phenylacetylene in the Ar or N_2 matrix and the formation of 1:1 complex of these species will be probed using infrared spectroscopy. Formation of these adducts will be evidenced by shifts in the vibrational frequencies of the acetylene and phenylacetylene monomers in the complex.

Introduction

The importance of hydrogen bonding cannot be overemphasized, as it influences many processes in physics, chemistry and biology. Hydrogen bonding is responsible for many of the unique properties of water and its consequent role as a solvent necessary for sustainability of life. The importance of hydrogen bonds and weak non covalent interactions in protein folding and DNA stability are also being studied and their roles delineated. According to the IUPAC definition, "The hydrogen bond is an attractive interaction between a hydrogen atom from a molecule or a molecular fragment X–H in which X is more electronegative than H, and an atom or a group of atoms in the same or a different molecule, in which there is evidence of bond formation."[1]

The energy of the hydrogen bonding interactions ranges from 10 kcal/mole for strong H-bonds to 1 kcal/mole for weak H bonds. Under the regime of weak H-bonds the C—H···π systems belong to a specific class. The C-H···π systems have gained a lot of attention because, unlike the case of conventional H-bonding where the hydrogen is attached to an electronegative atom, in this case the hydrogen is connected to a carbon system. Furthermore, in these systems rather than the electronegativity of the atom attached to hydrogen, the hybridization of the carbon atoms plays a significant role, as it determines the acidity of the hydrogens attached to it and its ability to form H-bonds. Secondly, in classical H bonds, the proton acceptor is an electronegative atom such as oxygen or nitrogen. However, in the C—H···π system the proton acceptor is the π electron system. The idea that π bonds could serve as proton acceptors in H-bonded interactions was first put forward by Dewar in 1944. [2] The π systems, whether they belong to aromatic systems or isolated double or triple bonds are associated with a negative charge density and hence are involved in a variety of intermolecular interactions with other electron deficient partner molecules. Knowledge of these interactions is crucial for understanding the complexity of chemical and biological systems. [3-5] The π--π and C—H···π interactions are present widely in variety of phenomena like crystal packing of molecules in the solid state [6,7], supramolecular encapsulation , molecular recognition, [8,9] host–guest interactions, functional nanomaterials, [10,11] formation of three-dimensional helical structures of DNA and RNA[12], intercalation of drugs in DNA[13] and protein folding and protein aggregation.[14,15]

Phenylacetylene is an interesting multifunctional molecule which presents competitive hydrogen bonding sites. In order to understand the hydrogen bonding interactions in multifunctional molecules, Patwari and co-workers have studied hydrogen-bonded complexes of phenylacetylene with various molecules such as water, methanol, ammonia and methylamine. As can be expected, phenylacetylene forms a variety of intermolecular structures which results from a fine balance of intermolecular forces.[16-18] For example, the phenylacetylene-methanol complex has a O-H· · ·π hydrogen bond, where the O-H group of methanol interacts with the π cloud of the benzene ring, similar to the complex of benzene-methanol complex.[17] Likewise, the phenylacetylene-methylamine complex is characterized by the presence of a N-H· · ·π hydrogen bond, with the N-H group of methylamine interacting with the π electron density of the benzene ring. On the other hand, phenylacetylene forms a linear C-H· · ·N, σ hydrogen-bonded complex with ammonia[18], which is very similar to acetylene-ammonia complex[19], whereas in addition, phenylacetylene forms a quasiplanar cyclic complex with water, involving O-H· · ·π and C-H· · ·O hydrogen bonds. Interestingly, in this complex the O-H group of a water molecule interacts with the π electron density of the C-C triple bond, while the C-H group of the benzene ring in the ortho position is hydrogen-bonded to the oxygen atom of the water molecule. Even though phenylacetylene has features of both benzene and acetylene, the structure of the phenylacetylene-water complex is different from both the benzene-water and acetylene-water complexes.[20,21] These results indicate that while studying interactions with multifunctional molecules, even small changes in the interacting partner can result in dramatic change in the intermolecular structure.

In general, it has always been a challenge to predict the behaviour of individual functional groups present in multifunctional molecules in the formation of weakly bonded complexes, such as the hydrogen bonded systems discussed above and π--π stacked systems.. Clearly, in a molecule with different functional groups, the nature of the weak complexes depends upon the competition between various interaction sites. The benzene dimer is the prototypical demonstration of π--π stacking which have been extensively investigated using both experimental and theoretical methods. There are various theoretical studies conducted on the benzene-dimer, ranging from very modest calculations to the more recent state-of-the-art calculations[22–36] .The two most important structural minima for the benzene-dimer are the slipped π -stacked and the C-H···π hydrogen-bonded T-shaped structures. The relative stability of the two minima depends

on the level of calculation employed. However, recent calculations at the CCSD(T)/CBS level indicates that both the π stacked structure and the T-shaped structures are almost isoenergetic.[30–34] In contrast to the number of theoretical studies, the number of experimental reports on the benzene-dimer are fewer.[37–42] The experimental evidence for the T-shaped geometry was provided by Arunan and Gutowsky, who using Fourier transform microwave spectroscopy analyzed the low J levels of the symmetric top system, with a large centrifugal distortion and a low barrier for internal rotation and proposed a T-shaped structure. Meijer and co-workers also proposed a tilted T-shaped structure based on the infrared spectra in the aromatic C–H stretching region.[42] More recent report by Patwari and co-workers on π stacked geometry of phenylacteylene dimer was observed using IR-UV double resonance spectroscopy in combination with ab initio calculations at the CCSD(T)/CBS level .The calculated stabilization energies and the free energies at this level favour the formation of an anti-parallel π stacked structure which was also confirmed from the observed IR spectra.[43]

In order to understand weak non covalent interactions, especially π-hydrogen bonded system and π--π interactions, we have chosen to study phenylacetylene and acetylene heterodimer, in this work. The prime motivation behind choosing this system is that phenylacetylene is a molecule with multifunctional sites for hydrogen bonding refers (Fig.1). It has two hydrogen bonding acceptor sites the benzene ring and the acetylenic C---C triple bond, and a proton donor site as the acetylenic C-H group. Similarly, acetylene has a C---C triple bond, which can act as proton acceptor, and an acetylenic C-H group, which can act as a proton donor. In the absence of strongly acidic or basic functional groups, the hierarchy of hydrogen sites cannot be determined on the basis of Etter and Legon-Millen rules.[44, 45]. It is a interesting to study this system, to understand the nature of the phenylacetylene-acetylene heterodimer. Since this system, is expected to present a number of minima on the potential surface, the problem turns out to be even more interesting. While in gas phase experiments the lowest energy complex is usually observed, the matrix isolation experimental technique that we have employed for this system is known to trap local minima. It was therefore interesting to see how many of these minima can be observed in the experiments.

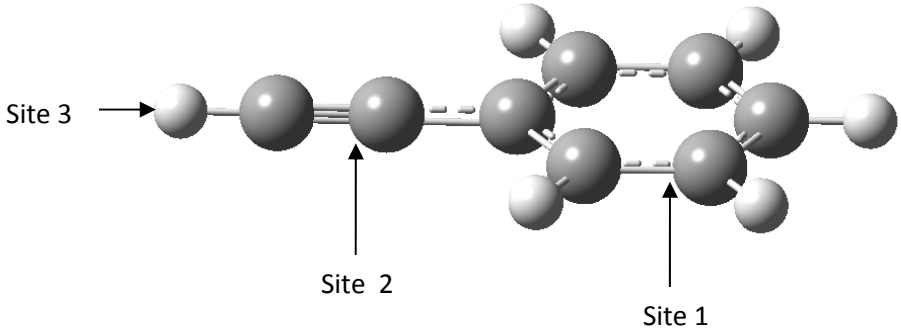

Phenylacetylene (PA)

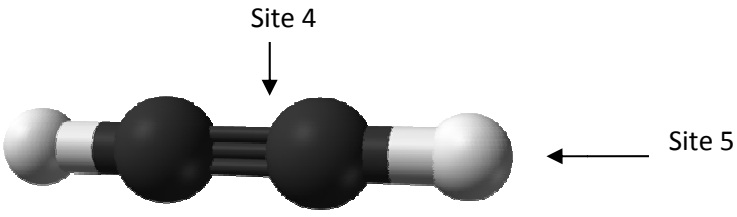

Acetylene (A)

Figure 1: The various hydrogen bonding sites in Phenylacetylene and Acetylene.

Chapter-2

2.1 EXPERIMENTAL SET UP AND COMPUTATIONAL PROCEDURES

This chapter describes the matrix isolation experimental setup and the computational methodology employed to study the hydrogen bonded complex between phenylacetylene (PA) and acetylene (AC).

2.1.1 Matrix isolation infrared spectroscopy

Matrix Isolation is an experimental technique in which guest molecules or atoms are trapped in rigid inert host materials.[46] It is a method of choice for the characterization of reactive intermediates and other unstable or transient species by spectroscopy as was first proposed and implemented by Pimentel.[47] In 1954, Pimentel and his co-workers developed the technique of matrix isolation, using inert gases to prepare the rigid matrix. This technique allows one to trap the reactive atoms or molecules in solid inert (or occasionally reactive) gases at a very low temperature range (4 - 40 K) see Fig. (2). The low temperature is achieved using a closed cycle helium cryostat and rigid matrices can be prepared using several non reactive noble gases or nitrogen, because of their nonreactive nature as well as their broad optical transparency in the solid state. Ar is commonly employed, while in a fewer cases, Ne, Kr or Xe are used. Performing experiments at cryogenic temperatures in an inert matrix ensures that line broadening due to collision and Doppler effect is minimized as the molecule are immobilized in the inert matrix.

Figure 2: A schematic showing the trapping of molecules, indicated by yellow/green gems in solidified inert matrix, shown by Almonds

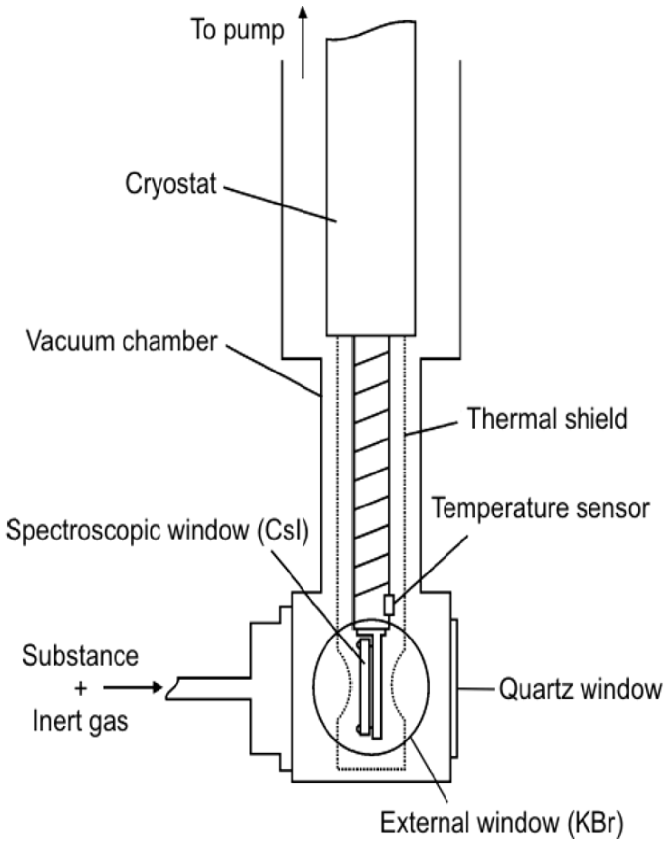

Figure 3: A schematic showing the cryostat required for attaining the cryogenic temperatures.

Matrices are formed by deposition of the inert gas and the sample of interest, on to a cold window such as the shown in Fig.3. Usually CsI, KBr and quartz windows are used as windows for IR and UV-visible studies, respectively, and copper or sapphire-tipped copper rods are used for ESR spectroscopy. The molecule under study must have a vapour pressure of a few millitorr at easily attainable temperatures (77 K to ~300K) so that it can be mixed with the inert gas by standard manometric techniques. It is an experimental challenge to deposit materials with exceedingly low vapour pressures, as using high temperatures for depositing such molecules, can often lead to decomposition of molecules.

In solid noble gas matrices, the interaction between matrix atoms and precursor molecules is weak. To avoid aggregation between isolated molecules, the samples are highly diluted (1000:1-10000:1) during the preparation of the matrix. The isolated molecules are trapped by the matrix cage so that the molecules cannot diffuse or rotate. In cases, where the sample under study is a liquid, it is degassed by freeze-pump-thaw cycles, before deposition. This is to ensure removal of any dissolved or entrapped air from the sample.

The temperature of the matrix must be below 30 % of the melting point of the noble gas used as the matrix (e. g. 30 K for Argon). Typical temperature of deposition is usually 10K, which is well below the limit mentioned above. Under these conditions, molecular diffusion is suppressed. When studying reactive species, these are produced in the matrix, using sources such as high pressure mercury lamp or laser. As it turned out the matrix isolation technique which was initially developed for studying reactive species had other benefits such as small line widths of spectral lines, which allowed for the study of weakly bonded complexes and conformations.

In matrix isolation experiments, the analyte molecules are isolated from each other in the cage of inert matrix atoms Fig.4, leading to the minimization of interaction between the analyte molecules. However, in principle the analyte molecule can interact with the matrix atoms but these interactions are weak. Complexities in the spectrum of a matrix isolated species arise due to a number of matrix effects, some of which are discussed in the subsequent section.

Figure 4: Shows the isolation of different molecules, shown as green and blue gems, in solidified inert Matrix (Almonds)

2.1.2 Matrix Effects

Understanding the various effects that matrix can have on the vibrational features of the analyte provides a basis for interpreting the infrared spectra of matrix isolated species. The most important effect is the perturbation of the vibrational modes of the molecule of interest due to the molecule-matrix interactions at any particular site. These interactions can result in either shift in the frequencies relative to isolated gas phase molecules, or splitting of the vibrational bands. The frequency shift, $\Delta\nu$, in a matrix with respect to the gas phase value arises from electrostatic ($\Delta\nu_{elec}$), inductive ($\Delta\nu_{ind}$), dispersive ($\Delta\nu_{dis}$) and repulsive interactions ($\Delta\nu_{rep}$) which is given by expression

$\Delta\nu = (\nu_{matrix} - \nu_{gas}) = \Delta_{velec} + \Delta_{vind} + \Delta\nu_{dis} + \Delta\nu_{rep}$ …. (2.1)

where, ν_{matrix} and ν_{gas} are the frequencies of the vibrational mode in the matrix and gas phase respectively.[46] Hence matrix shift gives important information about the interaction between the analyte and the matrix. In inert gas matrices, the long-range London dispersion forces and short range repulsive forces are the two dominant interactions. Pimentel and Charles have given a theoretical treatment of a matrix induced frequency shift.[47] The frequency shift, $\Delta\nu$, in solutions arising from the perturbation due to solvent interactions is given by the Buckingham expression

$\Delta\nu = (\nu_{solvent} - \nu_{gas}) = [Be/hc\omega e][U'' - (3aU'/\omega e)]$ …… (2.2)

where $Be = h/8\pi^2\mu cre$ is the rotational constant,

a = Anharmonicity constant,

U = Energy due to solute-solvent interaction,

$U' = \{\partial U/\partial r_{BC}\}$ and $U''= \{\partial^2 U/\partial^2 r_{BC}\}$, r_{BC} refers to the Fig.5 …… (2.3)

$c\omega e$ = Harmonic oscillator frequency for normal vibrational,

The above expression can be employed to explain the frequency shift occurring in the matrix. Fig.5 shows the interaction potential curves between the trapped molecule and matrix atoms when trapped in matrix cage. When R_{CM} is greater than R_1, i.e. when one of the atoms C, of the trapped molecule is more distant from the matrix atom, M, than R_e (equilibrium distance, Fig.5), U′ and U″ are negative and since ‘a’ is also negative, the term $\Delta\nu$ is negative (Eq. 2.2). Here the molecule experiences a loose cage effect inducing a negative frequency shift (red shift). When R_{CM} is less than R_e, U′ and U″ are positive and hence $\Delta\nu$ is positive. The molecule experiences a tight cage effect, which induces a positive frequency shift (i.e. blue shift). It was reported that when polyatomic molecules

are trapped in matrices, the high frequency stretching vibrations display negative shift as in a loose cage and the low frequency stretching, bending or rocking vibrations, give positive shifts as in a tight cage.47

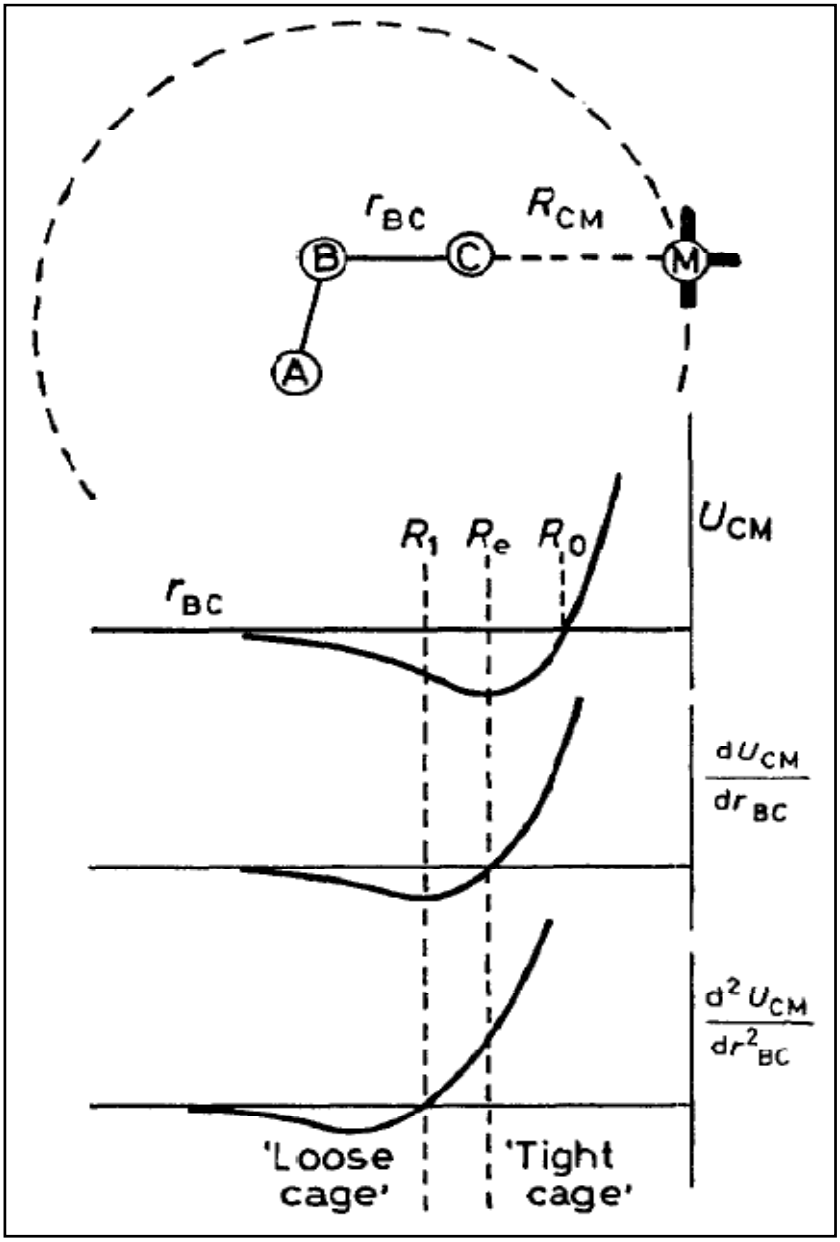

Figure 5– Plots showing the dependence of U, U′ and U″ on matrix cage size (Ref 47)

Apart from the shifts in the vibrational features, other factors which are likely to be responsible for multiple band structures in matrix are as follows

1) Rotation of the solute molecules in its trapping site,

2) Multiple trapping site effects,

3) Aggregation of the solute,

4) Lifting of degeneracy of the vibrational levels,

5) Inactive modes may also be induced.[49,50]

2.1.2.1 Rotation of analyte in matrix cage

Generally analyte species trapped in inert matrix cages at low temperatures, which hinders rotational motion, are rotationally inactive. However, rotations of a few small molecules become possible in noble gas matrixes having sufficiently large cavities. As a result, a number of small molecules, such as HX (X=F, Cl), H_2O, NH_3 and OH have been shown to rotate in noble gas matrixes. Although in general rotation seems not to occur in matrixes with unsymmetrical matrix sites, there are exceptions such as H_2 in a nitrogen matrix. Rotational features can be identified by reversible intensity changes when the matrix temperature is cycled. This reversible intensity variation occurs due to the change in population of rotational energy levels as the temperature is varied. Confirmation of these small molecules rotating in noble gas matrixes has been provided by observation of the pure rotational transitions in the far infrared or Raman spectrum[51-54].

2.1.2.2 Multiple trapping site effects

Different matrix sites perturb the vibrational potential differently and hence splitting in vibrational features is observed. It is possible that the analytes may be trapped in different types of sites in the matrix. Knowledge of these effects requires the knowledge of the geometrical structure of the cage of matrix atoms surrounding the trapped species.

The noble gas matrixes generally crystallize in cubic closed packed face centre cubic (f.c.c.) structure. A small amount of nitrogen or oxygen in solid argon can render a hexagonal close packed (h.c.p.) structure to be more stable. In f.c.c. structure, each atom is surrounded by 12 equidistant nearest neighbours and its symmetry is found to be an octahedron, O_h. The h.c.p. structure, which is less stable than the f.c.c. structure, also has 12 equidistant nearest neighbour, with a D_{3h} symmetry. The inert gases crystallize in f.c.c.

structure at cryogenic temperatures when no impurity is present. The closed packed lattices can have three possible guest sites; substitutional, in which the guest molecule is trapped by replacing one or more of the host species. Alternative, the guest molecule can also be trapped in interstitial sites, which have tetrahedral or octahedral symmetries. The geometry of these holes is of importance to matrix studies in relation to the perturbation, which the trapped species can experience. For example in a tetrahedral hole a small guest atom that is trapped would have four neighbouring matrix spheres arranged at the corners of tetrahedron. The radius of the small sphere that occupies the tetrahedral site is given by 0.225r, where r is the radius of the matrix sphere. Thus in order to occupy the tetrahedral site without disturbing the closed packed lattice, the radius of a trapped spherical species should be no larger than 0.225r. Similarly an octahedral site is surrounded by six close-packed spheres situated on the corners of an octahedron. The radius of an octahedral site is 0.414r. Usually, the most likely site is the substitutional site since it alone is large enough to accommodate most molecules of interest. The octahedral interstitial sites are much smaller than the substitutional sites but could conceivably accommodate smaller diatomic where as tetrahedral interstitial sites must be too small to be seriously considered. For example, small molecules such as H_2 and HCl, can occupy interstitial sites, which have a diameter less than 2 Å in argon or nitrogen matrix. For solute molecules trapped in different sites, each vibrational mode will exhibit more than one band since the interaction of the solute with the matrix environment will be different for different trapping sites. The relative intensity of multiplets due to different trapping sites is usually unaffected by solute concentration but can change on annealing at higher temperatures or by varying the rate of deposition.[55-58]

2.1.2.3 Aggregation

Isolation of the analyte is achieved only at a very high matrix/analyte (M/A) ratio, such as greater than 1000:1.At lower M/A ratios molecular aggregates may be trapped, in addition to the monomers. Molecular association will be greater for solutes capable of forming hydrogen bonds.[59,60] In contrast to liquids and solutions where broad absorption bands are usually observed, narrowing of bands occur on isolation in inert gas matrixes. Multiple features due to self-association can be readily identified from their concentration dependence and from warm-up experiments in which monomers diffuse to form dimer and higher multimers. The probability of isolation can be calculated as shown below for a molecule such as carbon monoxide, which occupies a single substitutional site. The

probability of interaction is simply the chance of finding another molecule occupying one of the 12 sites that form the cage. The chance for the absence of the second CO molecule is given by the formula $P = (1- r)^{12}$, where r is the reciprocal of the matrix ratio. For very small values of r the expression becomes, P = 1-12r. From this it is clear that a matrix ratio of 1000 is needed to ensure 99% isolation. It is found experimentally, for example, that carbon monoxide forms dimers or higher aggregates to the extent of several percent at a matrix ratio of 1000 in argon, rather than the1% expected on the basis of the analysis. Lithium atoms will dimerize completely even with matrix ratios of 10000 unless matrixes that rigidify at a very fast rate are used.[61,62] Aggregation can be eliminated by reducing the concentration of solute in the matrix. Matrix spectra should always be checked for concentration dependence to ensure that the bands are assigned to the correct species, i.e. the monomer, dimer or higher aggregate. Care has to be taken to check for possible impurity effects at lower concentrations.[63]

2.1.2.4 Lifting of degeneracy of vibrational levels

The symmetry of the site occupied by the molecule may also contribute to matrix effects. The perturbation of the molecule trapped in a particular site will be different for different vibrational modes leading to different frequency shifts. In case of degenerate vibrational modes, asymmetric sites can lead to a lifting of the degeneracy, resulting in the splitting of the vibrational features, such as that in CO_2 [64-66] and C_2H_2.[67,68] though both Ar and N_2 are commonly used as matrix materials, N_2 often interacts strongly with solutes in low temperature matrixes.[69,70]

2.1.3 Matrix isolation infrared setup

Important constituents of a matrix isolation set up are the following

(a) Cryostat (b) Vacuum system (c) Deposition lines for molecule introduction (d) Fourier transforms infrared spectrometer. Fig.6 describes the schematic of the matrix isolation setup.

A detailed description of the above components is illustrated below:

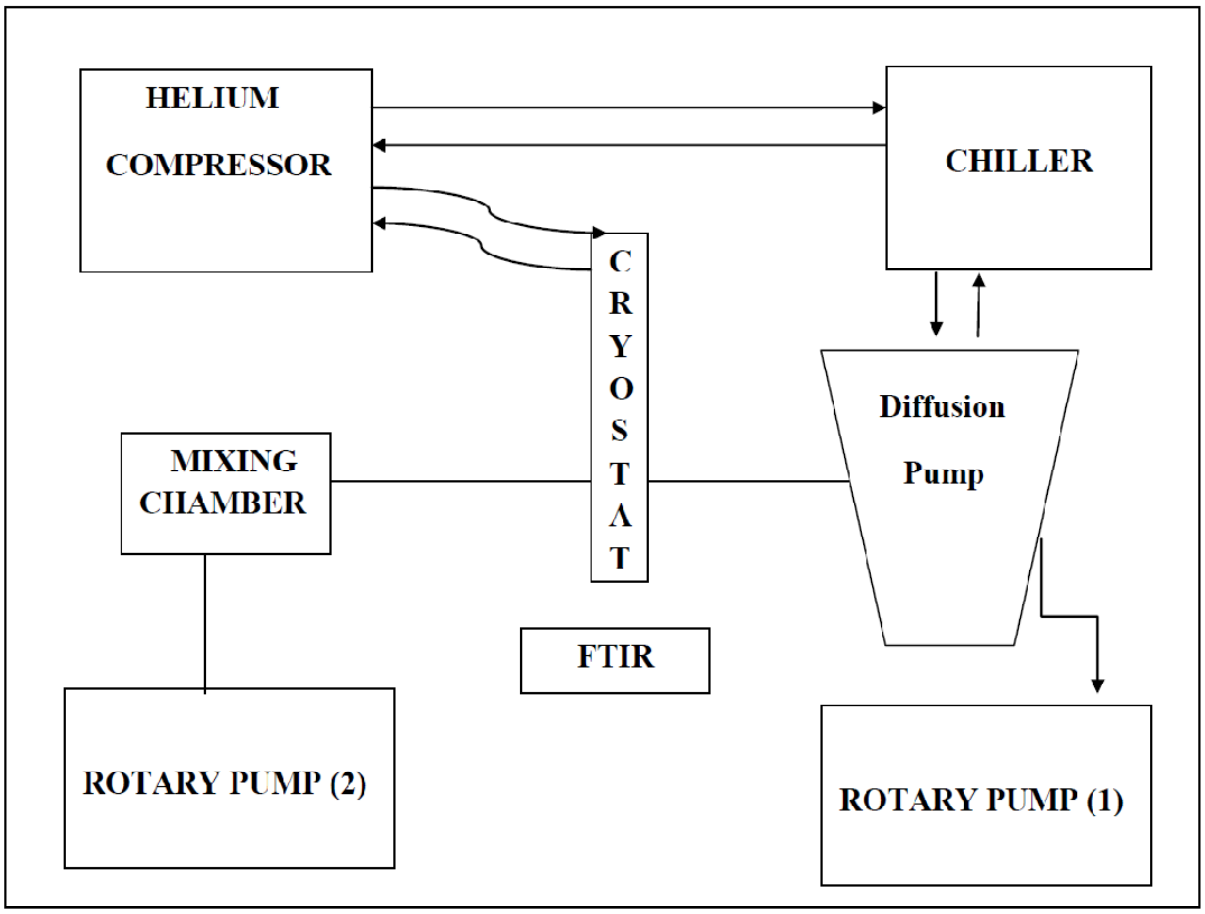

Figure 6 : Schematic block diagram of the matrix isolation setup

2.1.3.1 CRYOSTAT

The cryogenic temperature is required to solidify the inert gas to form the matrix and also to prevent diffusion of the trapped species. In order to achieve low temperatures as in 77K, 20K, 10K/K microrefrigerators with nitrogen, hydrogen and helium as working fluids respectively are widely available commercially. These microrefrigerators are also capable of going to higher temperatures by simply changing the rate of heat extraction which comes out to be very useful for controlled annealing and diffusion in the matrix. A closed cycle He cryostat was used in our set up and which is described below. There are other types of cryostats available like Joule Thomson and solvey cycle types[71] but they are not described here.

The closed cycle cryostat used in our set up works on the Gifford McMahon cycle. The important constituents of a closed cycle cryostat are the compressor, expander, vacuum shroud, and radiation shield. The expander, commonly known as the cold head or cold finger, is where the Gifford-McMahon refrigeration cycle takes pace. It is connected to a compressor through two gas lines for the working fluid (Helium) and an electrical power cable. One of the gas lines supplies high pressure helium gas to the expander, the other gas line returns low pressure helium gas from the expander. The compressor provides the necessary helium gas flow rate. The vacuum shroud surrounds the cold end of the expander in vacuum, limiting the heat load on the expander caused by conduction and convection. The radiation shield is actively cooled by the first stage of the expander and insulates the second stage from the room temperature thermal radiation being emitted from the vacuum shroud. Further, in addition to these major components, the closed cycle cryocooler is often accompanied by several support systems. Typically laboratory systems will have an instrumentation skirt, which provides a vacuum port and electrical feedthroughs, as well as a temperature controller to measure and adjust the sample temperature. The system also needs electricity, cold water for the compressor, and a vacuum pump for the sample space.

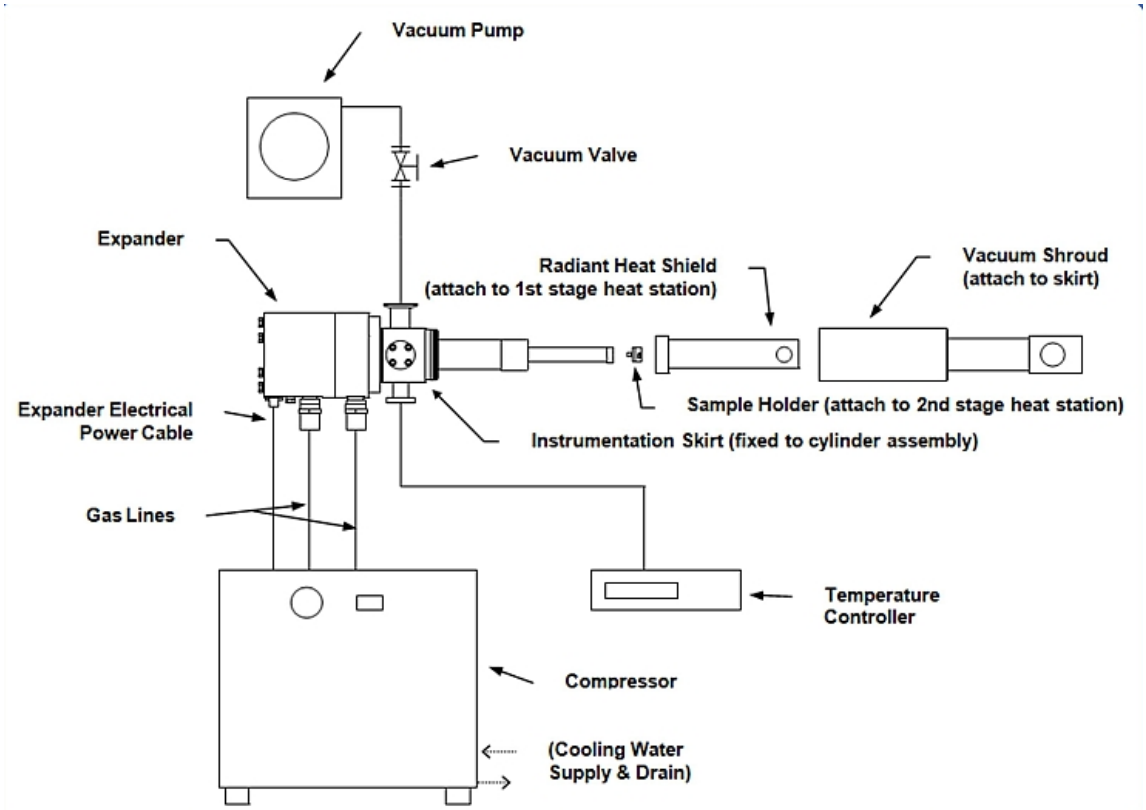

Figure 7:- Set up of closed-cycle Helium cryocooler Ref (72)

Grifford Mcmohan Refrigeration Cycle

The refrigeration cycle starts with the rotation of the valve disk opening the high pressure path allowing the high pressure helium gas to pass through the regenerating material into the expansion space. The pressure differential drives the piston "up" allowing the gas at the bottom to expand and cool. The rotation of the valve disk then opens the low pressure path allowing the cold gas to flow through the regenerating material removing heat from the system. Finally the pressure differential returns the displacer to its original position completing the cycle.

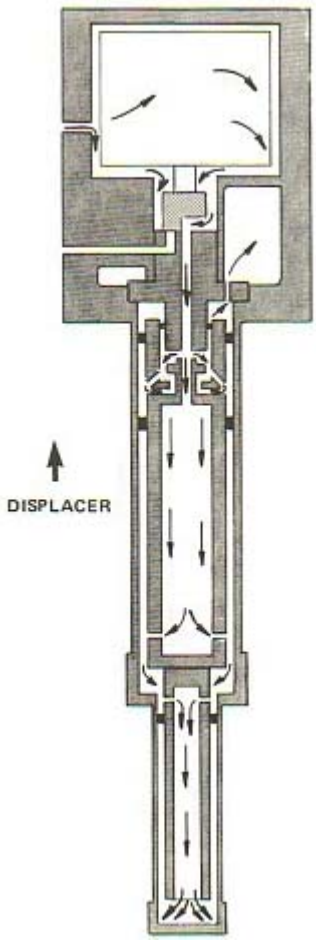

Figure 8: High pressure helium gas passing through the regenerating material into the expansion space Ref (72)

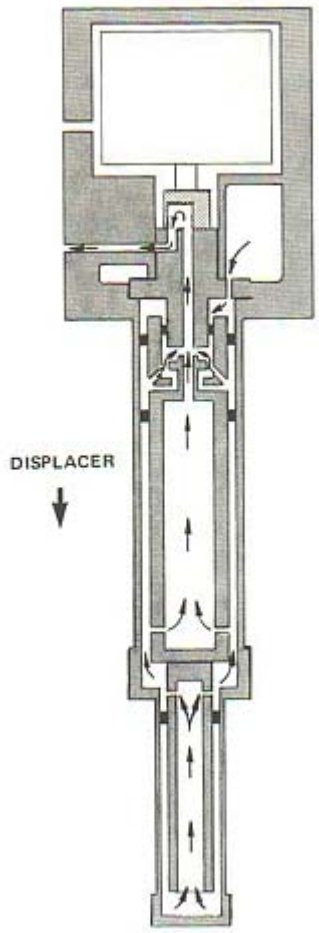

Figure 9: Low pressure valve opened allowing the cold gas to flow up through the regenerating material. Ref (72)

Our system is equipped with a closed cycle helium compressor cooled cryostat **CH-202w/HC4E1** Model (Sumitomo Heavy Industries Ltd.) which can attain a low temperature of 10K (Fig.10). The Helium compressor was cooled by a 3KW chiller unit which supplied cold water to remove the excess heat generated in the compressor.

Figure 10: Photograph of the helium compressor cooled cryostat CH-202w/HC4E1 in our experimental set up.

2.1.3.2 VACUUM SYSTEM

Vacuum pumps are classified based on the chemical or physical phenomenon that is responsible for pumping the gas molecules out of the vacuum vessel. Every vacuum pump operates in a limited pressure range and this range is limited by the vapour pressure of the materials of construction and the working fluids within the pump. Generally a pump which is operating in the viscous flow regime will not function in molecular flow region and vice-versa. In order to pump down a system to high vacuum from atmospheric pressures, two or more pumps are operated in series. In our setup, we have employed a mechanical rotary pump with a pumping speed of 200 L/m and vapour diffusion pump with a pumping speed of 300 L/s. The various accessories which were used in order to create an effective system are shown in the Fig.11.

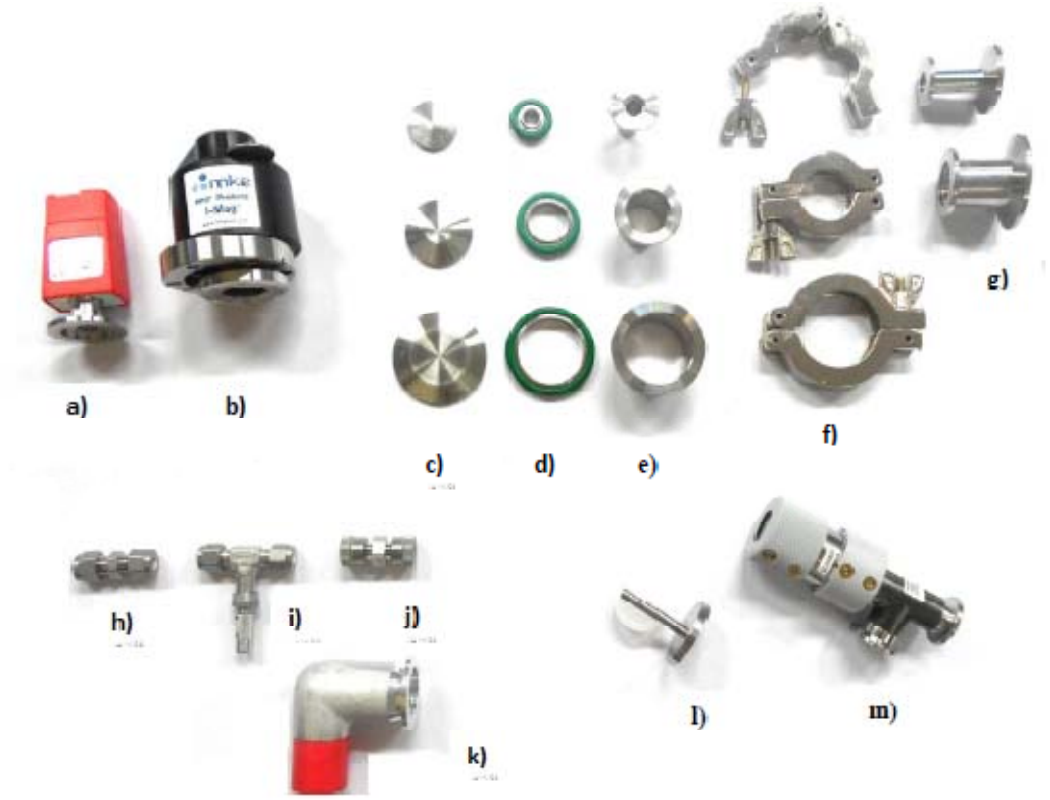

Figure (11): Photographs of the various vacuum components used in our setup. a)Pirani gauge b) Cold cathode gauge c) Dummy KF 40/25/10 d) O Rings KF40/25/10 e) KF 40/25/10 Flanges f) KF 40/25/10 Clamps g) KF 25-10,KF 40-25 Reducers h) Swagelok Straight fitting i) Swagelok metering valve (T shaped) j) Swagelok connectors k) KF 25 Right Angle Flange l) Single jet (effusive nozzle) m) High precision needle valve.

Mechanical Pump

Mechanical pump can pump down from atmospheric pressure down to a few mtorr. These pumps are essential to rough down a vacuum system to the required pressure before a high vacuum pump can be turned on. Furthermore, the mechanical pumps are also required for backing the high vacuum pump. The working of this pump is described below.

Oil-Sealed Rotary Vane Pumps –

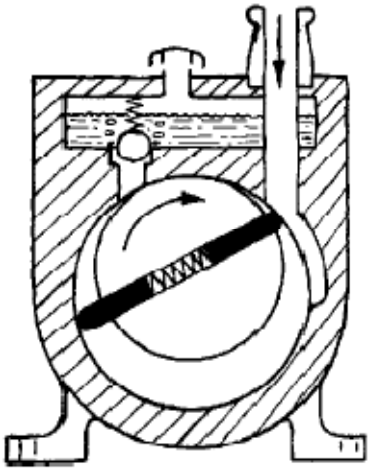

Figure 12: A schematic of an Oil- Sealed Rotary Vane Pump Ref(73)

These types of pumps are used mainly for obtaining pressures of a few millitorr. A rotary pump is schematically shown in Fig.11. In this pump a rotor turns off-centre within a cylindrical stator. The interior of the pump is divided into two volumes by spring-loaded vanes attached to the rotor. Gas from the pump inlet enters one of these volumes and is compressed and forced through a one-way valve to the exhaust. A thin film of oil maintains the seal between the vanes and the stator. The oil used is of good-quality hydrocarbon oil from which the high-vapour-pressure fraction has been removed. These pumps are also made in a two-stage version in which two pumps with rotors on a common shaft operate in series.

Rotary pumps which are to be used for pumping condensable vapours are provided with a valve known as gas ballast that admits air to the compressed gas just prior to the exhaust cycle. This additional air causes the exhaust valve to open before the pressures of

condensable vapours exceed their vapour pressure and thus prevents these vapours from condensing inside the pump. Rotary pumps are available with capacities of 1 to 500 L m^{-1} and are preferred as a backing pump for a diffusion pump.[73]

Vapour Diffusion Pump:-

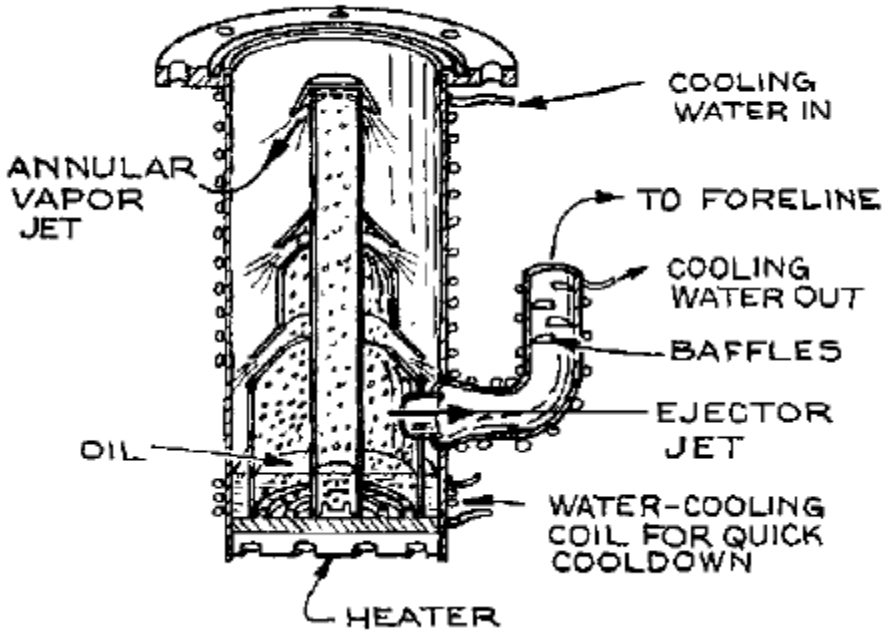

Figure 13: A schematic showing the working of the Diffusion Pump Ref (73)

Working of diffusion pump is based on momentum transfer to gas molecules from a directed stream of oil. As shown in Fig.14, the fluid (in our experiments silicon oil) is evaporated in an electrically heated boiler at the bottom of the pump. Vapour is conducted upward through a tower above the boiler to an array of thin nozzles from which the vapour is emitted in a jet directed downward and outward toward the pump walls. The diffusion pump walls are usually water-cooled so that molecules of the working-fluid vapour condense before their motion is randomized by repeated collisions. The chilled water is circulated from bottom to top in the tubings provided around the surface of the diffusion pump in order to avoid any void in between which will lead to lower cooling rate. The pumping action of a diffusion pump fails when the inlet pressure increases to the point where the mean free path of the molecules being pumped is less than the distance from the vapour-jet nozzle to the wall. When this happens the net

downward momentum of vapour molecules is lost and the vapour begins to diffuse upward into the vacuum system. Pumping of a vacuum chamber may be initiated at 50 to 100 mtorr. If this critical backing pressure is exceeded, the pump will stop and is said to have stalled. The usual practice is to maintain the oil-diffusion-pump foreline pressure below 50 mtorr. Silicone oils are the least expensive of the high-performance pump fluids. They are exceptionally resistant to oxidation and chemical attack, except in the presence of BCl_3 and, to a lesser extent, CF4 and CCl4.Other oils which are used with diffusion pumps are Octoil, Diffoil (di-2-ethylhexylphthalate) , and Santovac-5.[73] Diffusion pumps with speeds of 50 to 50000 L/s and with nominal inlet port diameters of 2 to 100 cm are available. Diffusion pump maintenance is less complicated as when the oil is opaque it is needed to be replaced. . The interior of the pump must be thoroughly cleaned before adding new oil Diffusion pumps use flat heating elements bolted to the bottom of the pump. A diffusion-pumped system is the most economical technique to obtain high and even ultrahigh vacuum in chambers of moderate size. With no moving parts and no critical dimensions, diffusion pumps are robust and long-lived.

Edwards Diffstak MK2 series diffusion pump was incorporated in our vacuum system, with a pumping speed of around 280 l/s for air, to attain the necessary vacuum. The diffusion pump was backed by a rotary pump with a capacity of 300 l/min. The base vacuum obtained with the above vacuum system was $\sim 10^{-6}$ mbar, measured using a cold cathode gauge (MKS vacuum Product I-Mag). For the effective working of the diffusion pump, it was cooled with chilled water at 15 °C, obtained using a 3KW chiller.

Figure 14: A photograph of the Edwards Diffstak MK2 series diffusion pump in our vacuum system.

Pressure Measurement:-

The pressure in a vacuum system may vary over many orders of magnitude and is usually measured using different types of gauges, appropriate for the different pressure regime. The gauges used in our vacuum system are described below:-

Capacitance Manometers - A capacitance manometer is a diaphragm manometer where the gauge head is divided into two chambers by a thin metal diaphragm that serves as one plate of a capacitor; the second plate of the capacitor is fixed in one of the chambers. A change in the pressure difference between the two chambers results in a change in capacitance as the flexible diaphragm moves relative to the fixed plate. A sensitive capacitance bridge measures the capacitance between the two plates and the capacitance is converted to a reading of the pressure difference. A capacitance manometer is designed so that the flexible diaphragm touches the opposing capacitor plate at a small overpressure. This protects the fragile diaphragm from a sudden thrust of gas. As might be expected, the capacitance measurement is very sensitive to the temperature of the flexible diaphragm. High precision gauge heads incorporate a heater and temperature control that maintains the gauge head at a constant temperature. Capacitance manometers are available to measure pressures from 1000 torr down to less than 10^{-4} torr.[73]

Thermal-Conductivity Gauges

The thermal conductivity of a gas decreases from some constant value above about 10 torr to essentially zero at about 10^{-3} torr.[73] This change in thermal conductivity is used as an indication of pressure in the Pirani gauge and the thermocouple gauge. In both gauges a wire filament is heated by the passage of an electrical current. The temperature of the filament depends on the rate of heat loss to the surrounding gas. In the Pirani gauge, the heated filament is one arm of a Wheatstone bridge. A change in temperature of the filament produces a change of resistivity and hence a change in the voltage across the filament. The resulting imbalance of the bridge gives an indication of pressure. Usually, a voltage is applied to keep the bridge in balance and this voltage serves as an indicator of the pressure. The pressure indicated by a Pirani gauge depends upon the thermal conductivity of the gas. They are usually calibrated by the manufacturer for use with air. For other gases these gauges must be recalibrated over their entire range, since thermal conductivity is a nonlinear function of pressure. This accuracy is adequate when the gauge is used to sense the foreline pressure of a diffusion pump or to determine whether the pressure in a system is sufficiently low to turn on a diffusion pump. The principal advantages of these gauges are ease of use, ruggedness, and low cost.

Ionization Gauges

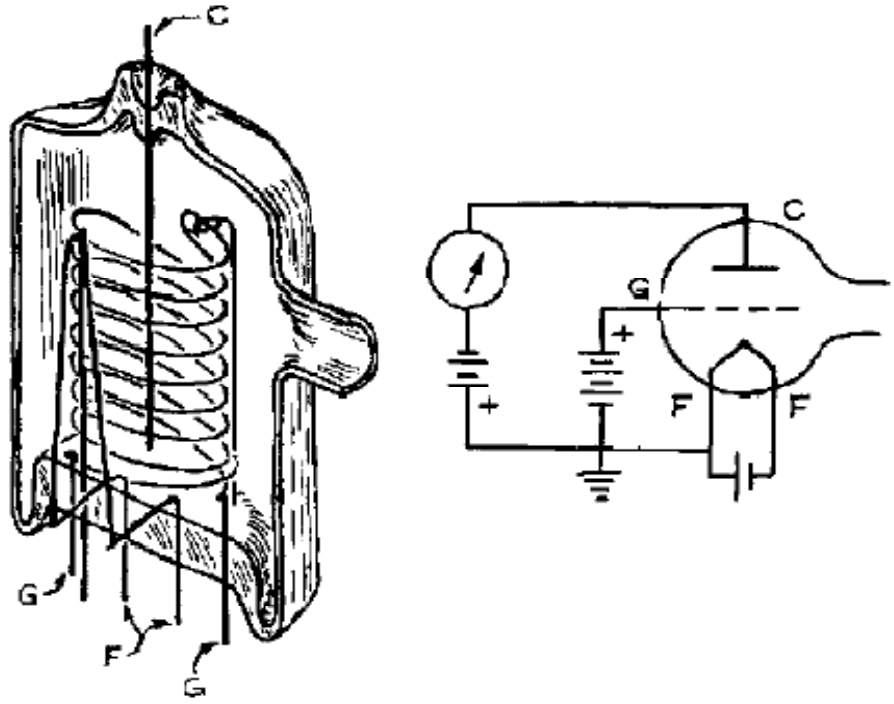

Figure 15: Working of a Cold cathode Gauge Ref (73)

In the cold cathode gauge an electrical discharge is struck in a low-pressure gas between two electrodes maintained at a potential difference of several kV. In order to provide the stability as well as to confine the path of the electron in the discharge, a magnetic field is applied in the gauge head. The discharge current measured at one of the electrodes provides a measure of the gas pressure. Cold cathode gauges operate in the 10^{-2} to 10^{-7} torr range with an accuracy of a factor of two at best.[73] Cold cathode gauges are robust and economical, suffering primarily only from their limited range of applicability. Cold cathode gauge in various configurations are referred to as Penning gauges, magnetrons and inverted magnetrons.

.

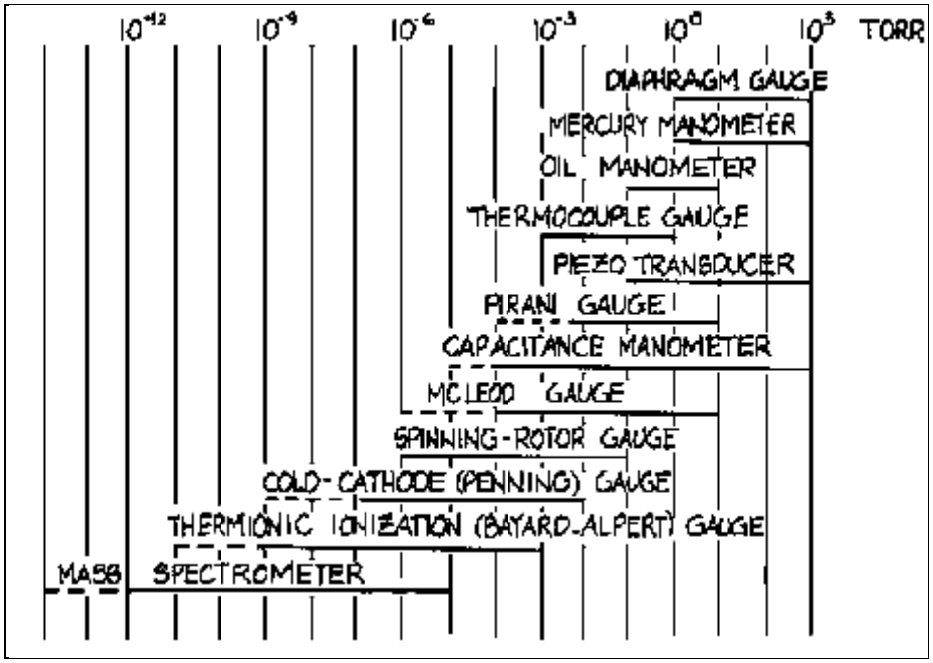

Figure 16: A Shows the working range of various gauges used in a vacuum system. Ref (73)

Figure 17: Pirani guage and Cold Cathode gauge

Fourier Transform Infrared Spectrometer (FTIR) -

The Vibrational spectra of the trapped molecules in the matrix were recorded using a Perkin Elmer FTIR spectrometer. This spectrometer is usually operated at a resolution of 1 cm^{-1} and typically 8 scans are coadded to obtain good signal-to-noise ratio. All spectra are recorded in the region of 4000 to 400 cm^{-1}. After the sample and matrix were deposited at 10 K, a spectrum of the matrix isolated species was recorded. After recording this deposition spectrum the temperature of the matrix was raised to around 30 to 35 K. The matrix was kept at this temperature for about 15-20 minutes using the heater-temperature controller unit (Lakeshore Instruments). The matrix was then again cooled back to 10 K and a spectrum was recorded. This process of heating the matrix followed by cooling is called Annealing. Annealing helps in removing unstable sites in the matrix as well as encourages diffusion of the precursor molecules to form adducts.

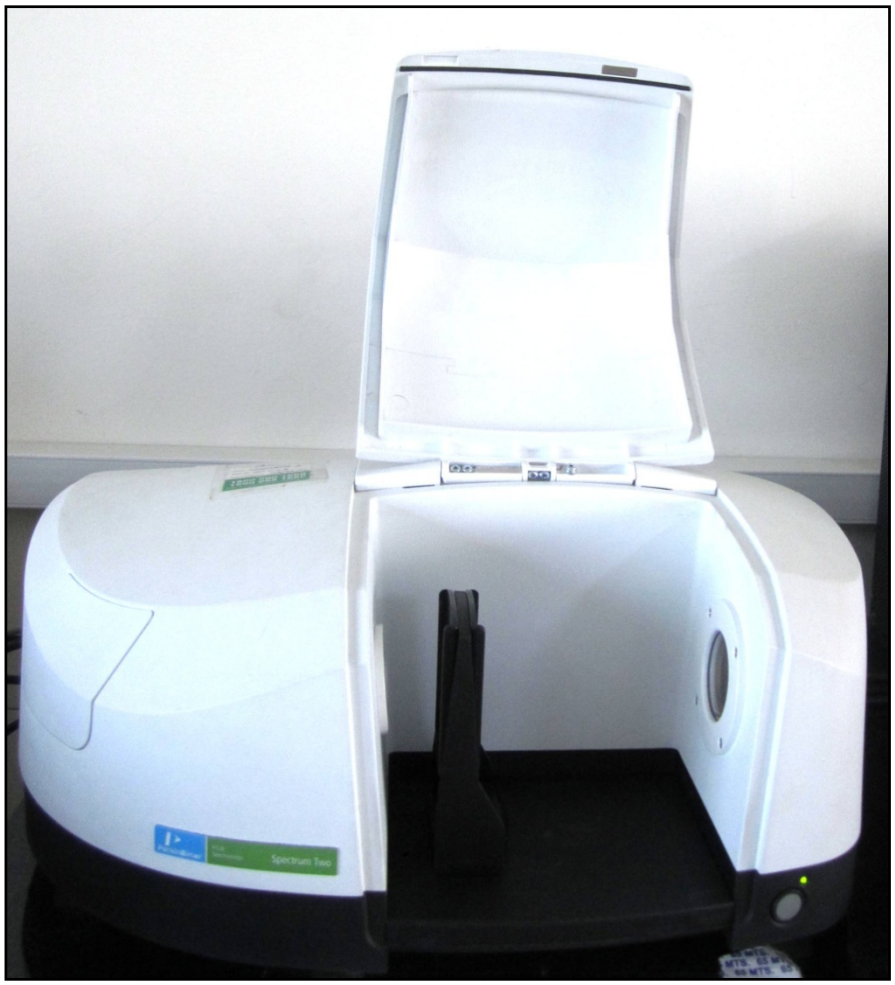

Figure 18: A photograph of the Fourier transform infrared spectrometer (FTIR)

2.1.3.3 ANALYTE INTRODUCTION

The basic requirement for conducting a MI experiment of a desired sample is that the compound should posses a vapour pressure large enough for deposition. For compounds which have a low vapour pressure are heated to a level to deposit them on the cold window whereas for compounds with high vapour pressure are cooled using liquid nitrogen and maintained at a particular temperature to get optimum vapour pressure. To start with a mixture of analyte and matrix was prepared in a stainless steel mixing chamber of one liter capacity, which was introduced to the vacuum system through a single effusive nozzle, also known as single jet nozzle. There are also other sources by which desired samples are introduced in the vacuum system namely- Double jet effusive nozzle and Hot nozzle source. In case where the analyte has low vapour pressure, deposition is carried out using a double jet nozzle system in which through one of the nozzles matrix gas is allowed to effuse out, while the second nozzle is used to introduce the sample into the vacuum system. On the other hand in order to identify the vibrational features for higher energy structures of the sample deposition was performed through a hot nozzle source, where the nozzle was maintained at various elevated temperatures.

2.1.4 Experimental procedure

The samples acetylene and phenylacetylene (Sigma Aldrich, 98% pure) were used for the study. The desired sample was loaded to the glass tubes connected to the system with the help of high vacuum glass stopcocks. Phenylacetylene, which is a liquid, was subjected to several freeze-pump-thaw cycles before use. Phenylacetylene has a vapour pressure of 1.46 torr at 0 °C, which is appropriate to obtain a matrix to sample ratio of 1000:1.Hence the sample was equilibrated in an ice-water mixture for about an hour, to obtain the desired vapour pressure over the sample. A stainless steel mixing chamber of one liter capacity was used to prepare matrix/sample gas mixtures. The mixture was deposited on the cold KBr substrate through single jet effusive nozzle. Speed of deposition was controlled by the help of a fine needle valve.

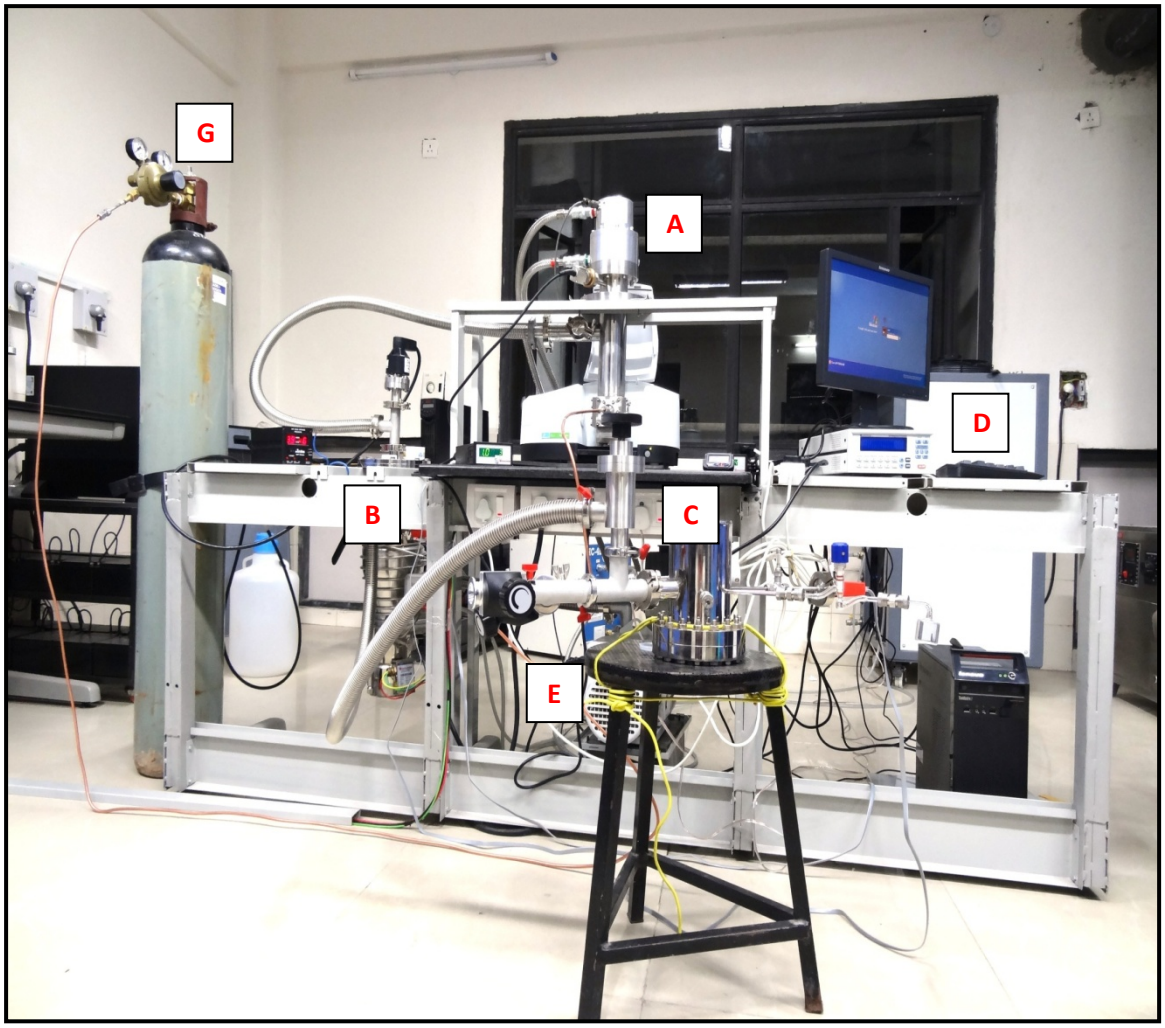

Figure 19: A photograph of the matrix isolation set up: A) Cryostat B) Diffusion Pump C) Mixing chamber D) Chiller E)Rotary Pump G)Nitrogen gas cylinder.

2.2 Quantum Chemical Computations

2.2.1 Geometry optimization and frequency calculation

At the outset, the structure of a molecule or complex corresponding to a minimum on the potential surface is achieved by geometry optimization. A geometry optimization protocol starts by making an initial guess of the molecular structure which is given as input. The energy and gradient are calculated at the point on the potential surface corresponding to the initial geometry and then this information is used to determine in which direction and to what extent the next step should be taken to improve the geometry. At the minimum in the potential energy curve all the forces will be zero. In the case of Gaussian software package the minimum energy structure of the molecules is achieved when the forces, the root mean square of forces, the calculated displacement and the root mean square of the displacement for the subsequent step are below specified threshold values. Geometry optimization calculations were performed at various levels of theories using Hartree-Fock (HF), Moller-Plesset second order perturbation (MP2) and Density functional methods (B3LYP,M05-2x,M06-2x) using a variety of basis functions. The B3LYP method uses the Becke three parameter non-local exchange functional[74,75] with non-local correlation of Lee et al.[76]

Vibrational frequency calculations were performed at the same level of theory which was used for optimization. The vibration computations were performed in order to confirm that the structures obtained indeed correspond to minimum in the potential surface and also to assign the vibrational features observed in the experiments. The computed vibrational frequencies were scaled to bring them in agreement with experimental results. In order to determine the scaling factor the experimentally observed strongest feature was correlated with the computed strongest feature. The scaling factor which would bring the computed frequency in good agreement with that of experiment was used to scale all other vibrational frequencies. Zero point vibrational energies (ZPE) were also obtained from the frequency calculation and which was used to calculate the ZPE corrected energies for the various complexes.

2.2.2 Stabilization energy calculation of complexes

The stabilization energy also referred to as interaction energy of the complex was calculated using the method described below. The stabilization energy (E) of a complex is given by

$E = E_{AB} - (E_A + E_B)$ ……. (2.4)

where, E_A, E_B and E_{AB} represent the energies for the monomers A, B and complex AB respectively. Negative value of E signifies that the complex is more stable relative to the precursors. The stabilization energy of the complex corrected for zero point energy (ZPE) was also calculated. When the energy of complex (E_{AB}) is computed, the basis functions used are those of both the monomer subunits. Whereas, for computing the energy of the individual precursors (i.e. E_A and E_B), the basis functions only corresponds to the precursors used. As the number of basic functions becomes larger in the computation of the complex, the energy obtained will be lower, due to the fact that each monomer can now use the basic functions of other. Stabilization energies thus derived from the calculated energies E_A, E_B and E_{AB} will be overestimated and the error is referred to as the basis set superposition error (BSSE).[77-81].The best way to eliminate the BSSE is to increase the basis set until the stabilization energy is the desired minimum with the tradeoffs of large computation times for even small systems. The commonly used method to correct for BSSE is through the use of the counterpoise correction method proposed by Boys and Bernadi. In this scheme, all the energies of monomer E_A, E_B and the complex E_{AB}, are computed in the same basis set spanned by the functions of the complex AB. The stabilization energies are then obtained as follows.

$E = E_{AB}(AB) - \{E_A(AB) + E_B(AB)\}$ …….. (2.5)

Where, $E_A(AB)$ = Energy of the monomer A using the basis set AB

$E_B(AB)$ = Energy of the monomer B using the basis set AB

$E_{AB}(AB)$ = Energy of the complex AB using the basis set AB

Zero Point Energy (ZPE) Correction

ZPE is the energy that a molecule posses even at absolute zero temperature. Stabilization energies to be experimentally meaningful must be corrected for the ZPE, as follows:

$\mathbf{E_{total} = E_{cal} + ZPE}$ …….. (2.6)

In our studies, the stabilization energies of the complex corrected for the BSSE have also been included. Corrections of energies for ZPE and BSSE simultaneously were not included as these values are known to overcorrect the stabilization values.[82,83].

2.2.3 Atoms-in-molecules (AIM) methodology

The atoms in molecules theory was first proposed by Bader which is based on electron density topology. For performing the (AIM) analysis the wave functions corresponding to the optimized geometry of a molecule or complex are generated using the Gaussian package.[84] From the electron density plot one can obtain the bond critical points, charge density ρ, Laplacian of charge density $\nabla^2\rho$, which is also the trace of the Hessian of ρ. The charge density, ρ(r), is a physical quantity which has a definite value at each point in space. Each topological feature of ρ(r), where it is a maximum, a minimum, or a saddle point, is associated with a space called a critical point, where the first derivative of ρ(r) vanishes. The sign of the second derivative at this point determine whether the function is maximum or minimum. The topological properties of such a scalar field are conveniently summarized in terms of the number and nature of its critical points. The rank of critical point, denoted by ω, is equal to the number of non-zero eigenvalues or non-zero curvature of ρ at the critical point. The signature denoted by σ, is the algebraic sum of the signs of the eigenvalues. The critical point (CP) is labelled by giving the values (ω, σ). For example, (3, -1) critical point means, three non-zero curvatures and one positive and two negative eigenvalues. A (3, -1) CP corresponds to a bond between two atoms, a (3, +1) CP to a ring, a (3, +3) CP to a cage and a (3, -3) CP corresponds to a maximum. The numbers of critical points of all types, which can coexist in a system with a finite number of nuclei, are governed by the Poincare-Hopf relationship.

$n - b + r - c = 1$ ……. (2.7)

where, n is the number of nuclei, b is the number of bond critical points, r is the number of ring critical points and c is the number of cage critical points.

The sum of three Hessians (λ1, λ2, λ3) at a bond critical point, the quantity $\nabla^2\rho$,provides a useful characterization of the manner in which the electronic charge density is distributed in the inter nuclear region. If the value of charge density ρ ($<10^{-1}$ au) and the curvature of charge density are large, Laplacian of charge density may be positive or

negative usually in the same order of magnitude as ρ then the interaction is of shared type, typical of covalent interaction. For the closed shell interactions, such as hydrogen bond complexes, van der Waals complexes and ionic systems, the charge density ρ ($\sim 10^{-2}$ to 10^{-3} au) at the bond critical point is quite small and the Laplacian of the charge density is positive.

Chapter 3: Results and Discussion

3.1 Computation

Phenylacetylene–Acetylene heterodimer was studied using both computational and experimental techniques. Experimentally, the hydrogen bonded complexes are proposed to be studied using matrix isolation which is a cold isolated molecule technique. The interest in phenylacetylene complexes stems from the fact that phenylacetylene has multiple sites for hydrogen bonding. It has one hydrogen donor and two hydrogen acceptor sites. On the other hand acetylene, the bonding partner has one hydrogen donor and one acceptor site. Hence this system was expected to show an interesting hydrogen bonding scenario, which is depicted in Fig 20.

The possible complexes which can be formed from the two monomers are listed below:-

1) Complex A - Hydrogen of acetylene acts as H-bond donor to the acetylenic π cloud in phenylacetylene.
2) Complex B - Acetylenic hydrogen of phenylacetylene acts as H-bond donor to π cloud in acetylene.
3) Complex C – Hydrogen of acetylene acts as H-bond donor to the π cloud of benzene in phenylacetylene.
4) Complex D – π-stacked geometry between π cloud of acetylene and π cloud of benzene in phenylacetylene.

The above four structures are intuitive, and the question that needs to be addressed is which of these four complexes represents the global minimum and if all the structures are indeed a minima on the potential surface. The optimization and frequency calculations were done at the various levels of theory of B3LYP, M05-2x, M06-2x, Moller Plesset Perturbation Theory (MP2), all using 6-311++g(d,p) basis set.

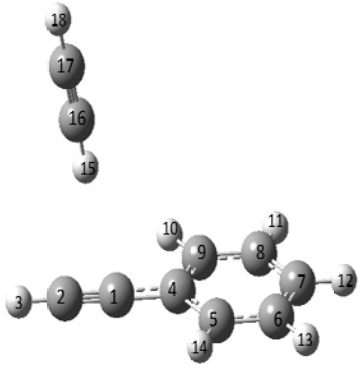

Complex1

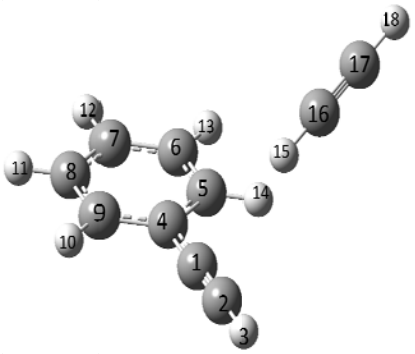

Complex1a*

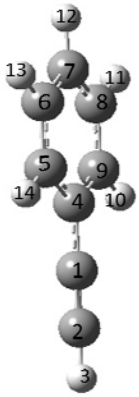

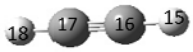

Complex2

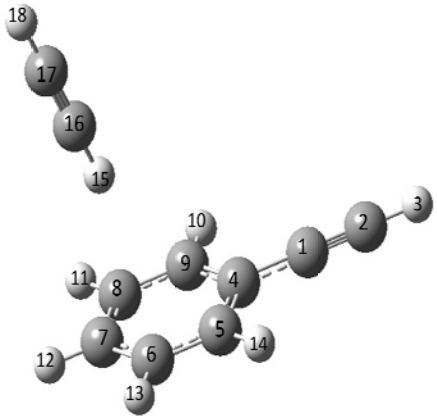

Complex3

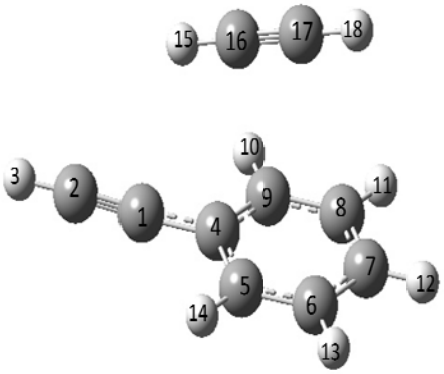

Complex4

Figure 20: Structures of optimized geometries obtained at MP2, M05-2X* and B3LYP using 6-311++G(d,p) basis set.

At the B3LYP/6-311++G(d,p) level of theory, three possible complexes were obtained which are shown in Fig.20; namely complex 1, complex 2 and complex 3. The intermolecular C-H distances were typically in the range of weak hydrogen bonds (2-3 A°).The important bond parameters for all three T-shaped complexes are indicated in Table 1. Stabilization energy of these complexes was computed after individually correcting for ZPE and BSSE (Table 2). At this level of theory Complex 1 is the most stable, followed by complex 2 and 3 , with interaction energies of -0.84,-0.64,-0.51 kcal/mole respectively. It must be noted that we have not reported the interaction energies, corrected for ZPE and BSSE together, since the combined application of both these corrections has been shown to overcorrect[82].

The frequency calculations were performed using the same basis set. All frequencies were found to be real, which confirms that the structures obtained were indeed minima on the potential energy surfaces. The various frequencies can be assigned to the monomers of the complex which are shown in (Table 3). When a proton donor molecule (X-H) approaches a suitable hydrogen bonding partner they form a hydrogen bond (X-H---Y) which results in an elongation of the X-H bond, and a resultant downshift of the ω(X-H) stretching vibrational frequency, and an IR intensity increase of the stretching vibration.[85] In all of the complexes obtained at this level, the C-H stretching modes of phenylacetylene and acetylene were red shifted. The magnitude of the red shift in complex 1 and 3 was larger for the acetylene monomer than phenylacetylene, as in these complexes acetylene served as proton donor. The C-H bending modes, on the other hand, were all blue shifted Fig.19.

AIM analysis

An examination of the charge density topology was performed using the atoms–in molecules (AIM) theory of Bader. (3, -1) bond critical points (BCP) and (3, +1) ring critical points (RCP) that could be associated with the complexes were located. The electron density ρ(rc) and Laplacian of electron density $\nabla^2\rho(\mathbf{rc})$ were computed for the critical points and the values are shown in Table 4. The ρ(rc) and $\nabla^2\rho(\mathbf{rc})$ values for bond critical points in the complexes were found to be in the order of 10^{-2} au . The large value of electron density for a critical point indicated the strength of the non covalent interaction present at the corresponding sites in the complexes Fig.20

Table 1 : Important structural complex parameters, bond lengths (Å), bond angles (°) and torsional angles[a] (°), of the various complexes (as indicated in Figure 20) of Phenyl acetylene and acetylene, computed at the B3LYP/6-311++G**

Complex Parameters	Complex 1	Complex 2	Complex 3
C1-C2	1.20	1.20	1.20
C16-C17	1.12	1.12	1.12
C16-C15	1.06		
C1-C15	2.94		
C2-H15	2.84		
C2-H3		1.06	
H3-C16		2.94	
H3-C17		2.94	
C4-H15			3.62
C7-H15			3.03
C16-H15			1.06
H15-C2-H3	97.76		
H15-C1-C4	106.72		
C1-C4-C5	120.48		
H3-C17-H18		102.12	
H3-C16-H15		101.89	
H14-C9-H10		0.00	
H15-C7-H12			103.42
H15-C4-C1			125.51
C1-C4-C9-H10			0.083
C17-C8-H11-H15			78.12
C17-C1-C4-C9		90.09	
C5-C4-C1-C15	85.75		
C1-C4-C5-H14	0.01		

[a]Torsional angle ABCD implies the angle between two planes ABC and BCD.

Table 2: Stabilization Energies (Kcal mol^{-1}) Raw/ZPE/BSSE corrected values

Complex	Interaction Energy			
	B3LYP/6-311++G(d,p)	**MP2/6-311++G(d,p)**	**M05-2X/6-311++G(d,p)**	**M06-2X/6-311++G(d,p)**
Complex 1	-1.03/-0.59/-0.84	-	-	-
Complex 1a	-	-	-2.28/-1.77/-2.11	-
Complex 2	-0.73/-0.38/-0.64	-2.25/-1.92/-1.10	-1.45/-1.13/-1.35	-1.38/-0.41/-1.28
Complex 3	-0.80/-0.47/-0.51	-4.50/-3.88/-2.00	-2.74/-2.23/-2.35	-2.95/-2.39/-2.59
Complex 4	-	-3.95/-4.12/-1.58	-2.01/-1.61/-1.80	-2.56/-2.11/-2.25

Table 3: Calculated Vibration Frequency shift (in cm^{-1}) and mode assignment for various Complexes at B3LYP/6-311G++(d,p).

Acetylene	**Complex 1**	**Δν***	**Complex 2**	**Δν***	**Complex 3**	**Δν***	**Mode Assignment**
772.92	791.46	18.54	774.40	1.48	781.77	8.85	out of the plane C-H bend
772.92	793.44	20.52	779.98	7.06	782.92	10	In plane C-H bend
3419.52	3399.48	-20.04	3416.56	-2.96	3410.90	-8.62	C-H Asymmetric stretch
Phenylacetylene							
644.50	653.38	8.88	696.28	51.78	649.61	5.11	out of the plane C-H bend
697.23	697.51	0.28	729.80	32.57	699.63	2.4	In plane C-H bend
772.25	774.25	2	772.53	0.28	773.53	1.28	C-H out of the plane bending in Benzene ring
3476.37	3472.51	-3.86	3449.00	-27.37	3476.36	-0.01	C-H stretch

Δν* = ν(computed complex)- ν(monomers)

Table 4: AIM calculations for the complexes obtained at B3LYP/6-311++G(d,p)

Complex	$\rho(rc)$ e/(bohr)^3	$\nabla^2\rho(rc)$ e/(bohr)^5
Complex 1	0.00492	0.01259
Complex 2	0.00379	0.01040
Complex 3	0.00554	0.01416

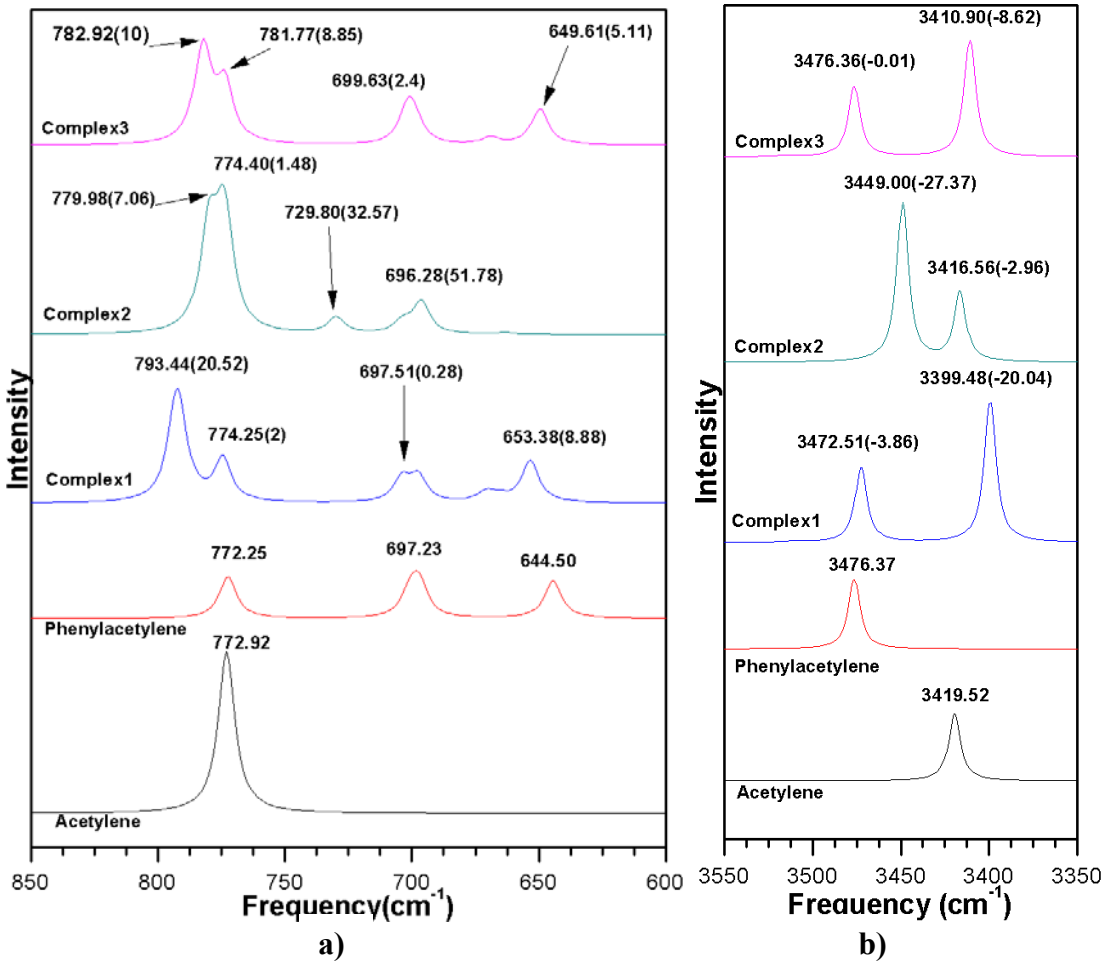

Figure 21 : Computed IR spectra of the various complexes in the region of the C-H bend (a) and stretch (b); obtained at B3LYP/6-311++g(d,p) level.

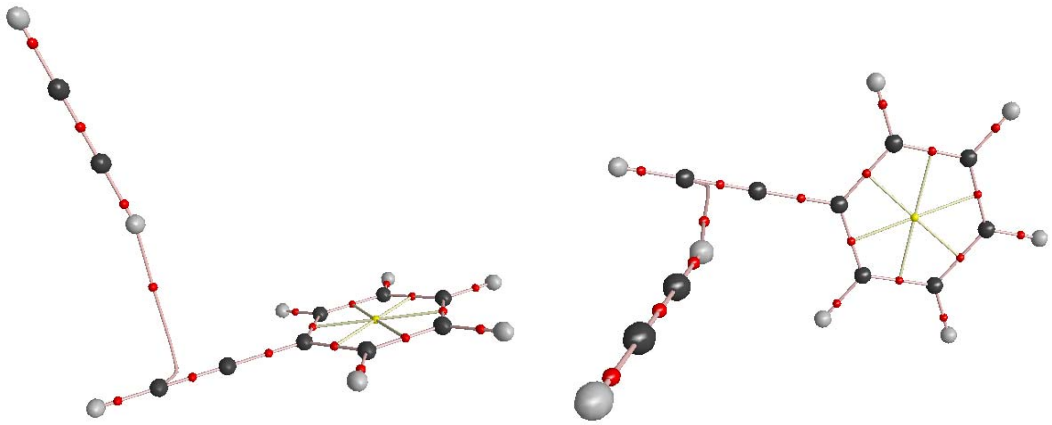

Complex 1

Complex 1a

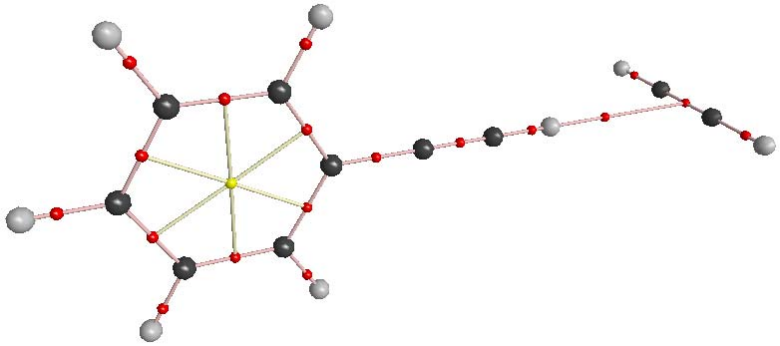

Complex 2

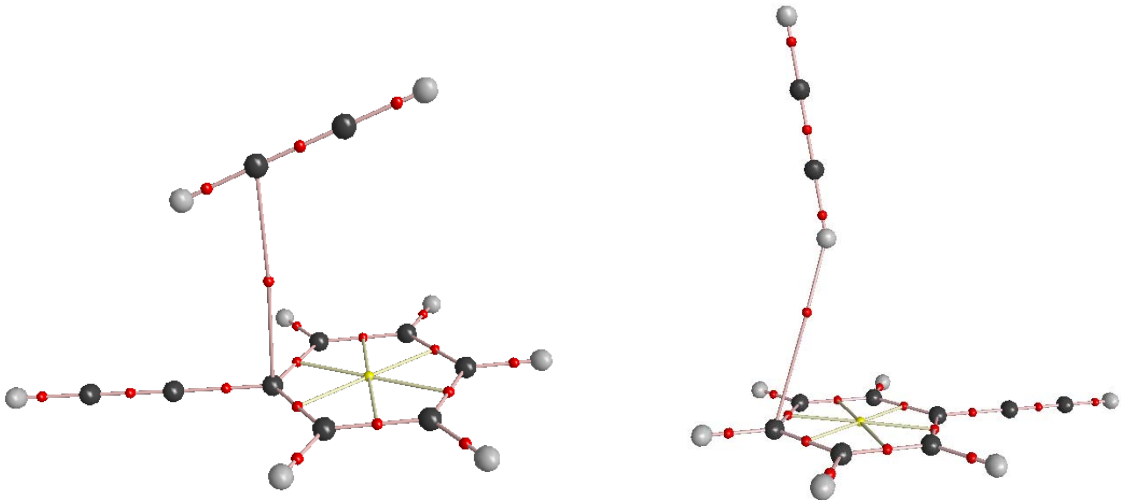

Complex 4

Complex 3

Figure 22: Structures of the complex showing the critical points obtained for all the complexes obtained at the B3LYP/MP2/M05/6-311++G(d,p)

Quantum chemical calculations at MP2/M05-2X/M06-2X levels of theory

As the B3LYP level is known not to reproduce weak non-covalent interactions accurately, computations were also done at the MP2 level of theory. The MP2 level of theory improves on the Hatree-Fork method by adding electron correlation effects by means of Rayleigh- Schrödinger perturbation theory (RS-PT) done at second order. Computation was done at this level of theory which yielded structures similar to Complex 2, Complex 3 and Complex 4. Interestingly, the most stable geometry obtained at the B3LYP/6-311++G** level, namely Complex 1, was not obtained at the MP2 level. Furthermore, a π-stacked structure was seen at the MP2 level, which was not obtained at the B3LYP level of calculations. Stabilization energy individually corrected for ZPE and BSSE was calculated for the various geometries (Table 2). The most stable complex was complex 3, followed by complex 4 and complex 2 with interaction energies of -2.00, -1.58, 1.10 kcal/mole respectively.

We have also performed computations on this system, using the Minnesota type hybrid functional such as M05-2X, M06-2X. Recent reports indicate that these hybrid functional better estimate non-covalent interaction, especially π- stacked and C-H---π interactions.[86,87] These computations were performed using the 6-311++G** basis sets.

At the M06-2X level, only three minima were obtained, which were similar to the results obtained at the MP2 level. The important bond parameters for all the three complexes are mentioned in the Table (5,7) . The increase in the C-H bond length in the complexes as compared with non complexed acetylene and phenylacetylene molecules indicates the presence of H-bonding interactions. In the stack geometry, the C1---C4 distance was 3.77 Å and 3.23 Å for MP2 and M06-2X, respectively. This bond distance lies in the range for typical π-stacked interactions. At the M06-2X level, the most stable complex was complex3, followed by complex4 and complex2, with interaction energies of -2.59, -2.25 and -1.28 kcal/mole respectively. The trend of the interaction energy remains almost same between MP2 and M06-2x levels. At M05-2X level four geometries were obtained, which were similar to those shown in Fig 1. Interestingly, the complex 1 structure which was found at this level was not identical with that obtained at the B3LYP level, but was somewhat different and is therefore labelled as complex 1a. Complex 1a obtained from M05-2X has the acetylene molecule situated at an angle of approx. 41° rather than 87° from the plane of the phenylacetylene as in the case of complex 1. The

differences in geometrical parameters are shown in the Table 9. At this level of theory, complex3 was the most stable form, followed by complex 1, complex4 and complex2; with interaction energies of -2.35,- 2.11,-1.80 and -1.35 kcal/mole respectively. Clearly the energy ordering obtained at this level is different from that obtained at the B3LYP level. The frequency calculations were performed for all the complexes at the different levels of theory (MP2, M06-2X, M05-2X). All frequencies were found to be real, which substantiate that the structures obtained were minima on the potential energy surfaces. Uniformly, the C-H stretching modes were red shifted in the both MP2/M06-2X level of computation with the acetylene C-H stretch being red shifted to a larger magnitude compared with the C-H stretch of phenylacetylene in complex 3 and 4 where the acetylene monomer served as the proton donor. Likewise, the phenylacetylene, which served as the proton donor in complex 2, showed C-H stretching modes red shifts which were larger than the acetylene modes see Fig.21 and 22. In the π-stacked structure, the C-H bending modes showed red shifts at both levels of computations. In contrast to the above frequency calculations, the M05-2x level showed that the C-H stretching modes of phenylacetylene in complex 1 and 2 were blue shifted but in complexes 3 and 4 these were seen to be red shifted Fig.23. In addition to this the π-stacked complex obtained at this level, showed all C-H bending modes to be blue shifted see Fig.25 , this was clearly different from what was obtained by M06-2X, MP2 level.

Table 5 – Important structural complex parameters, bond lengths (Å), bond angles (°) and torsional angles[a] (°), of the various complexes (as indicated in Figure 20) of Phenyl acetylene and acetylene, computed at the MP2/6-311++G**

Complex Parameters	Complex 2	Complex 3	Complex 4
C1-C2	1.22	1.22	1.22
C16-C17	1.22	1.22	1.22
C17-C7			3.88
C2-H15			3.34
C1-H15			2.96
C16-C4			3.77
C2-H3	1.06		
H3-C16	2.73		
H3-C17	2.73		
C4-H15		2.70	
C7-H15		2.77	
C16-H15		1.07	
H15-C1-C2			97.06
H15-C2-C4			79.64
C1-C4-C5			
C17-C7-H12			112.9
C17-C4-C1			110.01
H3-C17-H18	103.05		
H3-C16-H15	102.91		
H14-C9-H10	2.93		
H15-C7-H12		122.0	
H15-C4-C1		120.43	
C1-C4-C9-H10		1.04	1.67
C17-C8-H11-H15		91.46	
C17-C1-C4-C9	91.66		
C5-C4-C1-C15			
C1-C4-C5-H14			
C1-C4-C9-H15			75.77
C6-C7-C8-C16			83.91

[a]Torsional angle ABCD implies the angle between two planes ABC and BCD.

Table 6: Calculated Vibration Frequency shift in (cm^{-1}) and mode assignment for various Complexes at MP2/6-311G++ (d,p).

Acetylene	Complex 4	Δν*	Complex 2	Δν*	Complex 3	Δν*	Mode Assignment
765.06	755.19	-9.87	763.03	-2.03	804.01	38.95	out of the plane C-H bend
765.06	766.99	1.93	768.36	3.3	795.58	30.52	In plane C-H bend
3457.26	3449.50	-7.76	3452.13	-5.13	3453.17	-4.09	C-H Asymmetric stretch
Phenylacetylene							
620.81	612.63	-8.18	743.01	122.2	624.32	3.51	out of the plane C-H bend
679.90	671.59	-8.31	786.06	106.16	676.99	-2.91	In plane C-H bend
727.33	712.03	-15.3	709.98	-17.35	724.00	-3.33	out of the plane C-H bend in Benzene ring
3498.65	3495.71	-2.94	3476.26	-22.39	3497.52	-1.13	C-H stretch

Δν* = ν (computed complex) - ν (monomers)

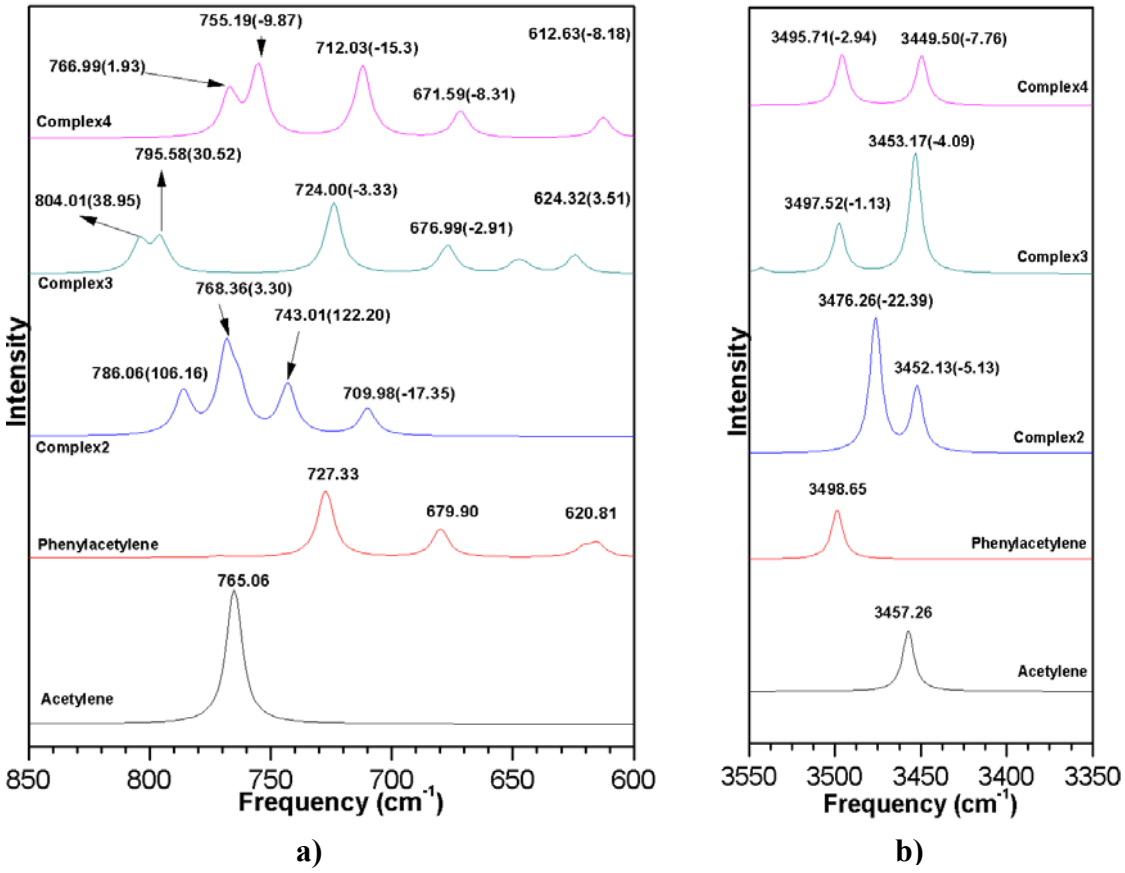

Figure 23: Computed IR spectra of the various complexes in the region of the C-H bend (a) and stretch (b); obtained at MP2/6-311++g(d,p) level.

Table 7– Important structural complex parameters, bond lengths (Å), bond angles (°) and torsional angles[a] (°), of the various complexes (as indicated in Figure 20) of Phenyl acetylene and acetylene, computed at the M06-2X/6-311++G**

Complex Parameters	Complex 2	Complex 3	Complex 4
C1-C2	1.20	1.20	1.20
C16-C17	1.19	1.19	1.19
C17-C7			3.89
C2-H15			3.27
C1-H15			2.87
C16-C4			3.23
C2-H3	1.06		
H3-C16	2.77		
H3-C17	2.77		
C4-H15		2.73	
C7-H15		2.91	
C16-H15		1.06	
H15-C1-C2			98.39
H15-C2-C4			59.52
C17-C7-H12			112.00
C17-C4-C1			107.76
H3-C17-H18	102.67		
H3-C16-H15	102.48		
H14-C9-H10	140.12		
H15-C7-H12		122.39	
H15-C4-C1		116.06	
C1-C4-C9-H10		0.00	1.74
C17-C8-H11-H15		55.89	
C17-C1-C4-C9	89.87		
C1-C4-C9-H15			73.50
C6-C7-C8-C16			55.36

[a]Torsional angle ABCD implies the angle between two planes ABC and BCD.

Table 8: Calculated Vibration Frequency shift (in cm^{-1}) and mode assignment for various Complexes at M06-2x/6-311G++ (d,p).

Acetylene	Complex 2	Δν*	Complex 3	Δν*	Complex 4	Δν*	Mode Assignment
794.90	796.63	1.73	804.08	9.18	805.83	10.93	out of the plane C-H bend
794.90	800.60	5.7	800.96	6.06	797.23	2.33	In plane C-H bend
3435.97	3431.24	-4.73	3424.06	-11.91	3424.43	-11.54	C-H Asymmetric stretch
Phenylacetylene							
693.14	743.57	50.43	698.95	5.81	691.98	-1.16	out of the plane C-H bend
705.47	705.64	0.17	781.54	76.07	704.57	-0.9	out of the plane C-H bend in Benzene ring
732.98	764.00	31.02	737.94	4.96	729.44	-3.54	In plane C-H bend
779.97	780.26	0.29	-	-	780.84	0.87	out of the plane C-H bend in Benzene ring
3495.72	3464.58	-31.14	3494.24	-1.48	3494.15	-1.57	C-H stretch

Δν* = ν (computed complex) - ν (monomers)

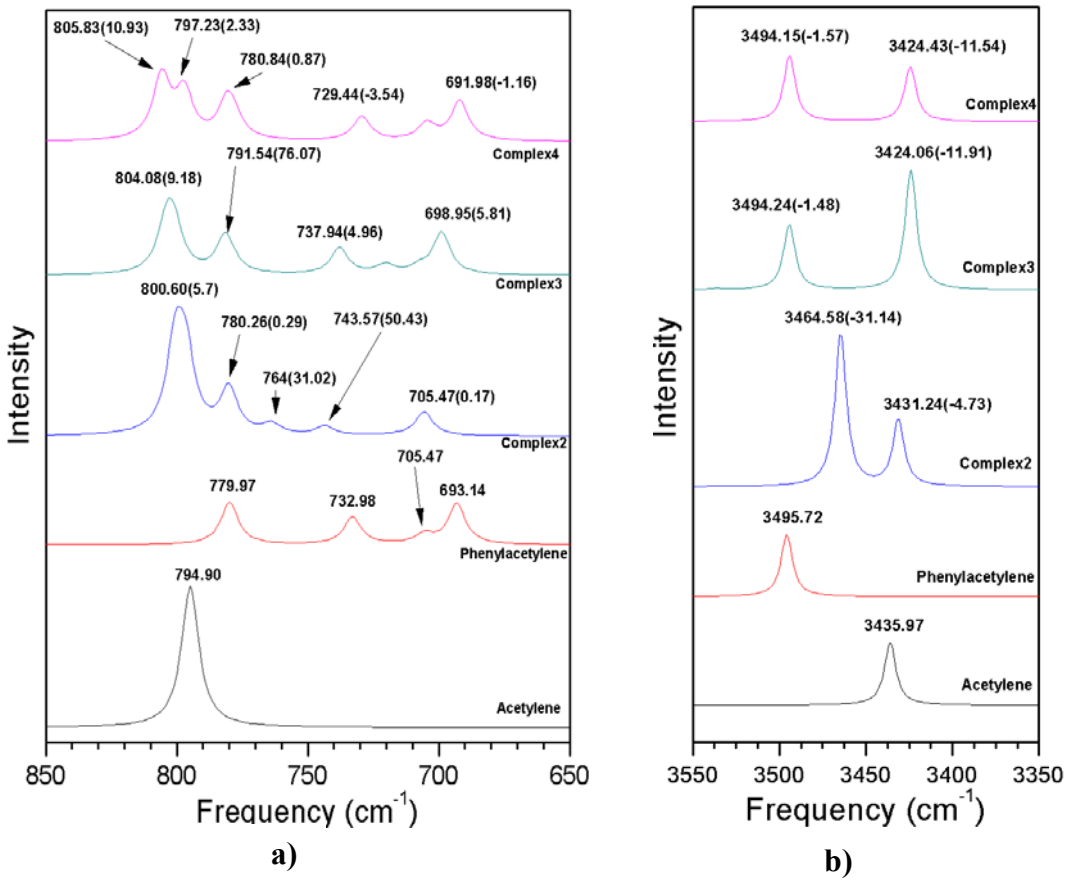

Figure 24: Computed IR spectra of the various complexes in the region of the C-H bend (a) and stretch (b); obtained at M06-2X/6-311++g(d,p) level.

Table 9 – Important structural complex parameters, bond lengths (Å), bond angles (°) and torsional angles[a] (°), of the various complexes (as indicated in Figure 20) of Phenyl acetylene and acetylene, computed at the M05-2X/6-311++G**

Complex Parameters	Complex 1	Complex 2	Complex 3	Complex 4
C1-C2	1.20	1.20	1.20	1.20
C16-C17	1.19	1.19	1.19	1.19
C17-C7				4.70
C2-H15	2.80			3.04
C1-H15	2.68			2.70
C16-C4				3.42
C2-H3	1.06	1.06		
H3-C16		2.79		
H3-C17		2.78		
C4-H15			2.81	
C7-H15			2.89	
C16-H15	1.06		1.06	
H15-C1-C2				95.02
H15-C2-C4				61.11
C17-C7-H12				116.83
C17-C4-C1				97.40
H3-C17-H18		102.43		
H3-C16-H15		102.02		
H14-C9-H10		140.10		
H15-C7-H12			122.34	
H15-C4-C1	96.680		117.73	
H15-C1-C4	108.60			
C1-C4-C9-H10	0.15		0.17	1.18
C17-C16-C9-C8			91.59	
C17-C1-C4-C9		90.04		
C1-C4-C9-H15				69.60
C6-C7-C8-C16				52.35
H14-C5-C4-H15	41.49			

[a]Torsional angle ABCD implies the angle between two planes ABC and BCD.

Table 10: Calculated Vibration Frequency shift in (cm^{-1}) and mode assignment for various Complexes at M05-2x/6-311G++ (d,p).

Acetylene	Complex 1	Δν*	Complex 2	Δν*	Complex 3	Δν*	Complex 4	Δν*	Mode Assignment
786.90	802.38	15.48	789.89	2.99	796.61	9.71	812.17	25.27	out of the plane C-H bend
786.90	809.04	22.14	793.55	6.65	796.12	9.22	801.19	14.29	In plane C-H bend
3466.02	3443.45	-22.57	3461.60	-4.42	3454.12	-11.9	3451.42	-14.6	C-H Asymmetric stretch
Phenylacetylene									
693.57	701.25	7.68	745.65	52.08	693.71	0.14	694.85	1.28	out of the plane C-H bend
710.27	712.13	1.86	710.86	0.59	712.54	2.27	711.42	1.15	out of the plane C-H bend in Benzene ring
734.18	738.37	4.19	766.47	32.29	732.31	-1.87	737.89	3.71	In plane C-H bend
785.76	788.10	2.34	785.19	-0.57	788.28	2.52	788.03	2.27	out of the plane C-H bend in Benzene ring
3524.13	3557.54	33.41	3568.88	44.75	3520.79	-3.34	3520.39	-3.74	C-H stretch

Δν* = ν (computed complex) - ν (monomers)

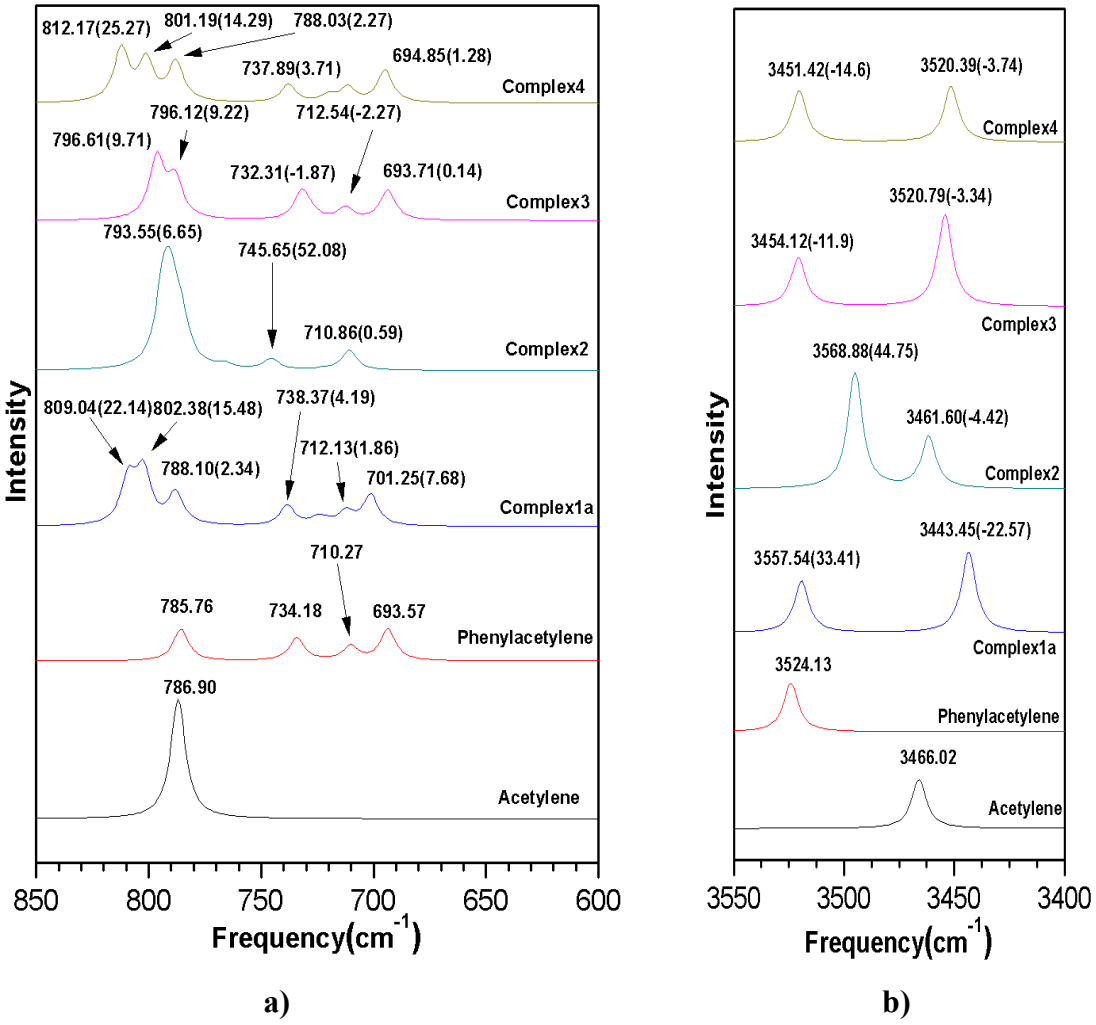

Figure 25: Computed IR spectra of the various complexes in the region of the C-H bend (a) and stretch (b); obtained at M05-2X/6-311++g(d,p) level.

AIMS calculation for MP2/M05-2X/M06-2X levels of theory

Intermolecular interactions present in the phenylacetylene-acetylene heterodimer was examined by applying the atoms-in- molecule (AIM) theory of Bader to the optimized geometries. This method is based on the analysis of electron density topology. This method is very useful for indentifying and characterizing weak hydrogen bonds. A The critical points for each of the complexes at various levels were found and are showed in the Fig.20.The ρ(rc) and $\nabla^2\rho$**(rc)** values for bond critical points in the complexes were also found to be in the order of 10^{-2} au . The large value of electron density for a critical point indicated the strength of the non covalent interaction present at the corresponding sites in the complex. Table (11, 13)

Table 11: AIM calculations for the complexes at the MP2/6-311++G (d,p).

Complex	**ρ(rc) e/(bohr)^3**	**$\nabla^2\rho$(rc) e/(bohr)^5**
Complex 2	0.00712	0.02058
Complex 3	0.00727	0.02479
Complex 4	0.00728	0.02184

Table 12: AIM calculations for the complexes at the M06-2X/6-311++G (d,p)

Complex	**ρ(rc) e/(bohr)^3**	**$\nabla^2\rho$(rc) e/(bohr)^5**
Complex 2	0.00658	0.01812
Complex 3	0.00673	0.02104
Complex 4	0.00716	0.02195

Table 13: AIM calculations for the complexes at M05-2X/6-311++G (d,p)

Complex	$\rho(rc)$ e/(bohr)^3	$\nabla^2\rho(rc)$ e/(bohr)^5
Complex 1a	0.00727	0.02031
Complex 2	0.00643	0.01711
Complex 3	0.00594	0.01810
Complex 4	0.00641	0.02004

3.2 Experiments

Matrix isolated infrared spectrum of water and phenylacetylene was recorded using a nitrogen matrix at ~12 K employing the newly established MI setup. The details of the experimental procedures are described below.

a) Matrix Isolated Infrared Spectrum of Water

Nitrogen was filled (~700 torr) in the mixing chamber through a quarter inch copper tubing connected to the nitrogen cylinder. This was followed by deposition of nitrogen on to the cold substrate KBr window at ~12 K. The rate of flow of the gas was controlled by a high precision needle valve connected between the mixing chamber and cryostat. Deposition was done using a flow rate of ~3mmol/hr for about an hour. After deposition, the infrared spectrum was recorded in transmission mode with a resolution of 1.0 cm^{-1} and 8 scans at 12 K. A matrix isolated spectrum of water in a nitrogen matrix was recorded. The stretching modes of water were observed at 3727.1 and 3634.6 cm^{-1} corresponding to antisymmetric and symmetric O-H stretch. The O-H bend was located at 1597 cm^{-1} see Fig.26. The matrix was annealed progressive at 20, 25 and 30 K. It was observed that on annealing, the features of the water monomer decreased and new features at 3715.3, 1601 cm^{-1} were observed, which were due to the water dimer in the matrix.[88] The peak values found were in close amenity with the reported frequency values for water monomer and dimer. The experiments confirmed the successful working of the MI setup.

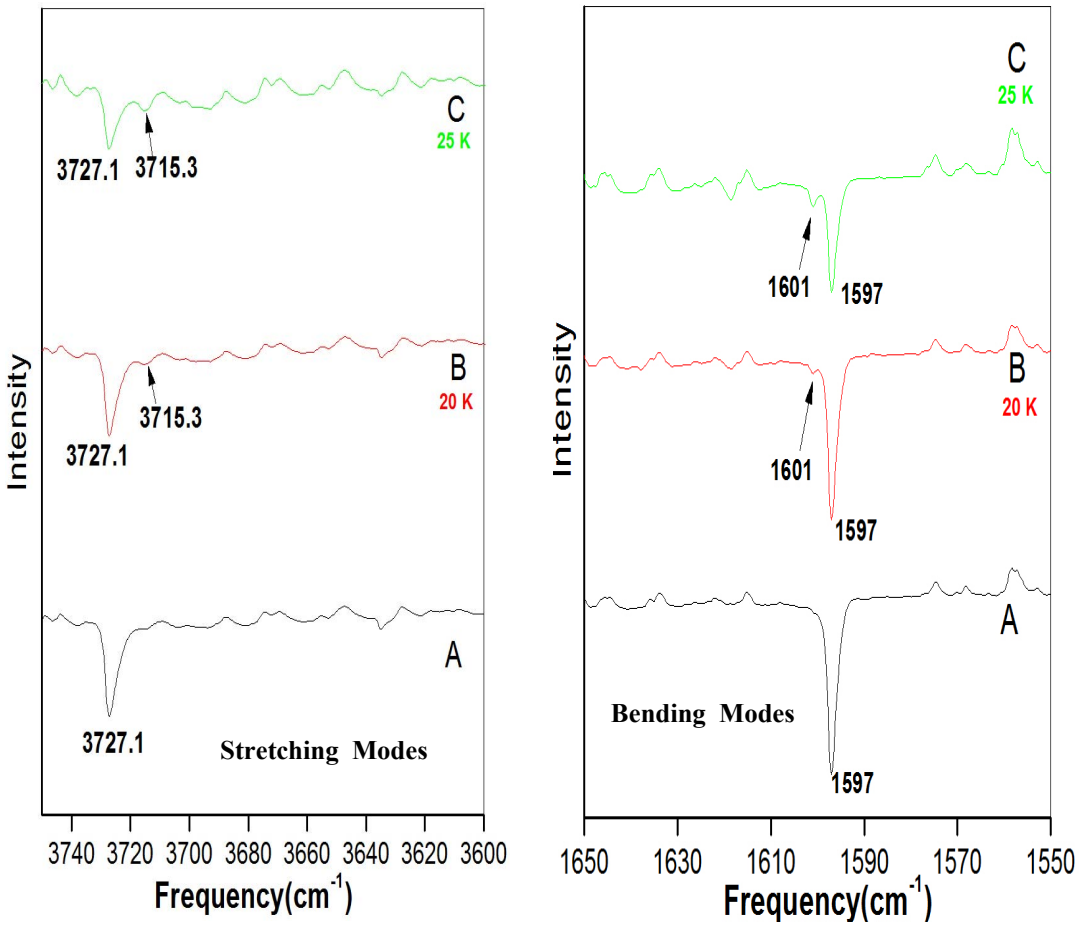

Figure 26 : Matrix isolated IR spectra of water in N_2 matrix at 12K (A) followed by annealing at 20/25K (B/C)

b) Comparison of Phenylacetylene Matrix Isolated spectra with the liquid IR spectrum

Phenylacetylene (99% pure Sigma Aldrich) was taken in the sample holder tube and then was subjected to several freeze-pump-thaw cycle before mixing with nitrogen to avoid other volatile impurities present in the sample. Phenylacetylene was cooled to 0°C in order to have a vapour pressure of ~ 1.45 torr. The vapour pressure at this temperature was calculated using the vapour pressure data of Phenylacetylene as reported by Steele and co-workers[89] .The temperature of the sample was maintained at 0°C for about 25 mins, to ensure equilibration. Phenylacetylene was then mixed with nitrogen at an approximate matrix to sample ration of 1000:1, and deposited on the KBr window kept at 12 K. The spectrum was recorded at 12 K followed by annealing at 30K.Liquid

Phenylacetylene spectrum was also recorded and was compared with the matrix isolated spectrum. The broad vibrational features in the liquid spectrum became sharper as shown in Fig.27.

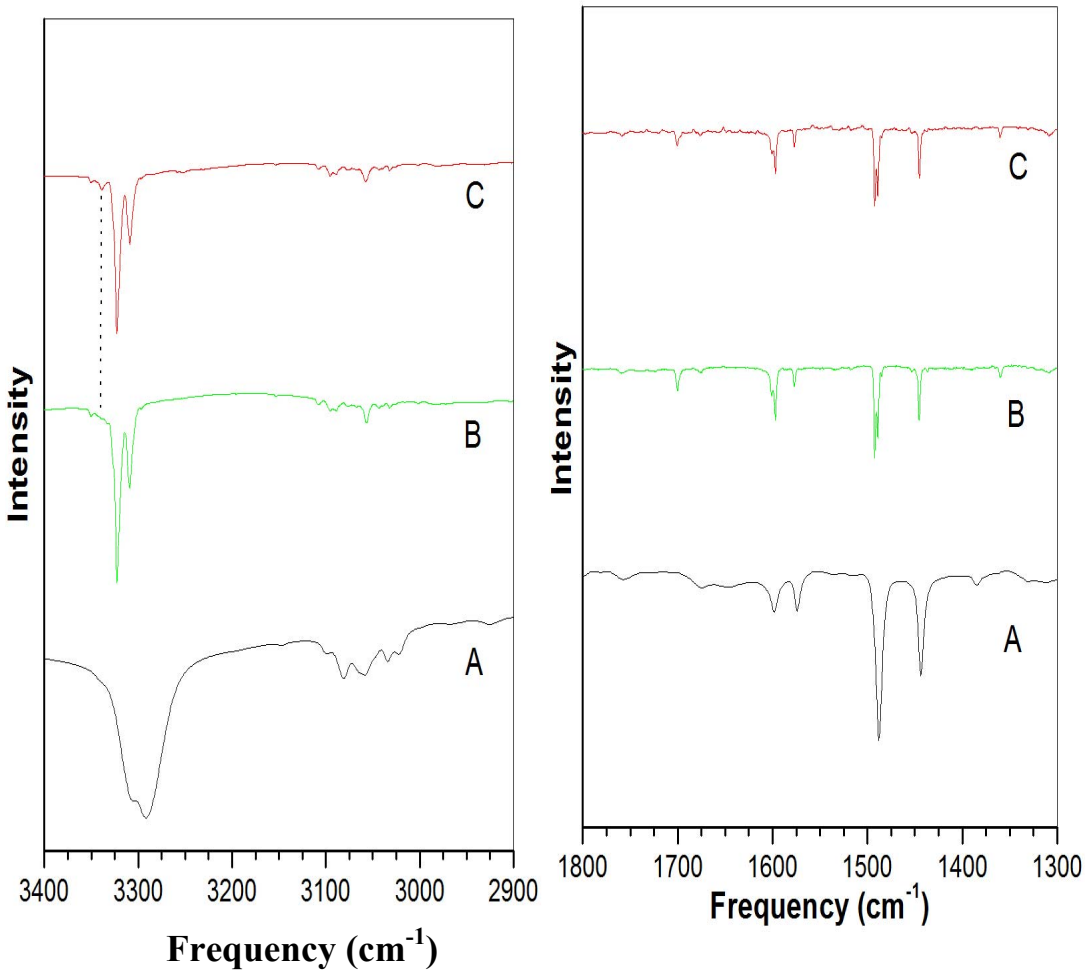

Figure 27 : Shows (A) Liquid IR spectrum of Phenylacetylene compared with (B) Matrix isolated spectra at 12K; (C) Annealed spectrum at 30K .

3.3 Conclusions

Matrix isolation infrared spectroscopic technique well known for trapping transient species and investigating extensively weak non covalent interactions was successfully established during the course of the MS-project. A vacuum of approximately 3 x 10^{-6} torr was achieved with the help of the Edwards diffusion pump backed by oil sealed rotary pumps. Helium compressor cooled cryostat mounted on a steel frame was utilized to bring the temperature down to 10K. At this temperature the host molecules are rigid with very limited degrees of freedom. Helium compressor and diffusion pump were cooled by a 3KW water chiller with the temperature maintained at 15-16°C. Phenylacetylene and nitrogen were commixed in a mixing chamber at matrix to sample ratios of 1:1000 and deposited on the cold KBr window using single jet effusive source. Matrix isolation infrared spectrum for two molecules phenylacetylene and water was recorded. The DFT calculations involving the B3LYP hybrid functional gave three T shaped structures as optimized geometries, where the complex1 was the most stable least energy structure, but at higher level of calculations where electron correlation was better emphasized like M06-2X and MP2, π-stack geometry was seen with complex 3 as the most stable among the possibly obtained optimized geometries. The M05-2X DFT functional gave rise to both complex 1 and stack geometry complex 4, where the structure with least energy was complex 3 followed by complex1 and at the end the stack geometry. The difference between the energy ordering at various levels of calculations will be better comprehended by performing requisite experiments.

Bibliography

1) Elangannan Arunan, Gautam R. Desiraju, Roger A. Klein,Joanna Sadlej, Steve Scheiner, Ibon Alkorta, David C. Clary,Robert H. Crabtree, Joseph J. Dannenberg, Pavel Hobza,Henrik G. Kjaergaard, Anthony C. Legon, Benedetta Mennucci,David J. Nesbitt, Pure Appl. Chem., 2011,83,1619–1636.

2) Dewar, M. J. S. *J. Chem. Soc*. 1944, 406

3) G.C. Pimental, A.L. McClellan, The Hydrogen Bond, W.H.Freeman, San Fransisco, 1960.

4) G.A. Jeffrey, W. Saenger, Hydrogen Bonding in Biological Structures, Springer, Berlin, 1991.

5) J.E. Del Bene, in: P.v.R. Schleyer (Ed.), Encyclopedia of Computational Chemistry, Wiley, New York, 1998.

6) J. Bernstein, R. E. Davis, L. Shimoni, N. L. Chang, Angew. Chem. 1995,107, 1689 – 1708; Angew. Chem. Int. Ed. Engl. 1995, 34, 1555– 1573.

7) S. L. Childs, P. A. Wood, N. Rodriguez-Hornedo, L. S. Reddy, K. I. Hardcastle,Cryst. Growth Des. 2009, 9, 1869 –1888.

8) A. Iwasaki, A. Fujii, T. Watanabe, T. Ebata, N. Mikami, J. Phys. Chem. 1996, 100, 16053 –16057.

9) A. Fujii, T. Ebata, N. Mikami, J. Phys. Chem. A 2002, 106, 10124 – 10129

10) T. Ebata, A. Fujii, N. Mikami, Int. Rev. Phys. Chem. 1998, 17, 331 –361.

11) P. Imhof, W. Roth, C. Janzen, D. Spangenberg, K. Kleinermanns, Chem.Phys. 1999, 242, 153 –159.

12) S. H. Dale, M. R. J. Elsegood, A. E. L. Coombs, CrystEngComm 2004, 6,328 –335.

13) P. Imhof, W. Roth, C. Janzen, D. Spangenberg, K. Kleinermanns, Chem Phys. 1999, 242, 141 –151.

14) B. Brutschy, Chem. Rev. 2000, 100, 3891 –3920.

15) U. Spoerel, W. Stahl, J. Mol. Spectrosc. 1998, 190, 278– 289

16) Singh, P. C.; Bandyopadhyay, B.; Patwari, G. N. J. Phys. Chem. A 2008, 112, 3360.

17) Singh, P. C.; Patwari, G. N. J. Phys. Chem. A 2008, 112, 5121.

18) Singh, P. C.; Patwari, G. N. J. Phys. Chem. A 2008, 112, 4426

19) Fraser, G. T.; Leopold, K. R.; Klemperer, W. J. Chem. Phys. 1984,80, 1423.

20)(a) Engdahl, A.; Nelander, B. *J. Phys. Chem.* 1985, *89*, 2860. (b)Wanna, J.; Menapace, J. A.; Bernstein, E. R. *J. Chem. Phys.* 1986, *85*,1795. (c) Suzuki, S.; Green, P. G.; Bumgarner, R. E.; Dasgupta, S.; Goddard,W. A., III; Blake, G. A. *Science* 1992, *257*, 942. (d) Pribble, R. N.; Garrett,A. W.; Haber, K.; Zwier, T. S. *J. Chem. Phys.* 1995, *103*, 531. (e) Gutowsky,
H. S.; Emilsson, T.; Arunan, E. *J. Chem. Phys.* 1993, *99*, 4883.

21) (a) Engdahl, A.; Nelander, B. *Chem. Phys. Lett.* 1983, *100*, 129.(b) Peterson, K. I.; Klemperer, W. *J. Chem. Phys.* 1984, *81*, 3842.

22) M. O. Sinnokrot, E. F. Valeev and C. D. Sherrill, J. Am. Chem.Soc., 2002, 124, 10887.

23) O. M. Sinnokrot and D. C. Sherrill, J. Phys. Chem. A, 2006,110, 10656.

24) S. Tsuzuki, K. Honda, T. Uchimaru, M. Mikami and K. J. Tanabe, J. Am. Chem. Soc., 2002, 124, 104.

25) W. Wang, M. Pitonak and P. Hobza, ChemPhysChem, 2007,8, 2107.

26) R. A. Distasio Jr.,G. vonHelden, R. P. Steele andM. Head-Gordon,Chem. Phys. Lett., 2007, 437, 277.

27) J. Rezac and P. Hobza, J. Chem. Theory Comput., 2008, 4, 1835.

28) O. Bludsky, M. Rubes, P. Soldan and P. Nachtigall, J. Chem.Phys., 2008, 128, 114102.

29) S. Tsuzuki, T. Uchimaru, M. Mikami and K. Tanabe, Chem. Phys.Lett., 1996, 252, 206.

30) T. Janowski and P. Pulay, Chem. Phys. Lett., 2007, 447, 27.

31) R. A. Distasio, G. von Helden, R. P. Steele and M. Head-Gordon,Chem. Phys. Lett., 2007, 437, 277.

32) E. C. Lee, D. Kim, P. Jurecka, P. Tarakeshwar, P. Hobza and K. S. Kim, J. Phys. Chem. A, 2007, 111, 3446.

33) M. Pitonak, P. Neogrady, J. Rezac, P. Jurecka, M. Urban and P. Hobza, J. Chem. Theory Comput., 2008, 4, 1829.

34) M. O. Sinnokrot and C. D. Sherrill, J. Am. Chem. Soc., 2004,126, 7690.

35) A. von Avoird, R. Podeszwa, K. Szalewicz, C. Leforestier,R. von Harrevelt, P. R. Bunker, M. Schnell, G. von Helden andG. Meijer, Phys. Chem. Chem. Phys., 2010, 12, 8149.

36) P. Hobza, H. L. Selzle and E. W. Schlag, J. Am. Chem. Soc., 1994,116, 3500.

37) K. C. Janda, J. C. Hemminger, J. S. Winn, S. E. Novick, S. J. Harris and W. Klemperer, J. Chem. Phys., 1975, 63, 1419.

38) M. Steed, T. A. Dixon and W. Klemperer, J. Chem. Phys., 1979,70, 4940.

39) K. O. Biirnsen, H. L. Selzle and E. W. Schlag, J. Chem. Phys.,1986, 85, 1726.

40) B. F. Henson, G. von Hartland, V. A. Venturo, R. A. Hertz and P. M. Felker, Chem. Phys. Lett., 1991, 176, 91.

41) E. Arunan and H. S. Gutowsky, J. Chem. Phys., 1993, 98, 4294.

42) U. Erlekam, M. Frankowski, G. Meijer and G. von Helden,J. Chem. Phys., 2006, 124, 171101.

43) Surajit Maity, G. Naresh Patwari, Robert Sedlak, Pavel Hobza ,*Phys. Chem. Chem. Phys.,* 2011, **13**, 16706–16712

44) (a) Etter, M. C. *Acc. Chem. Res.* 1990, *23*, 120. (b) Etter, M. C. *J.Phys. Chem.* 1991, *95*, 4601.

45) Legon, A. C.; Millen, D. J. *Chem. Soc. Re*V. 1987, *16*, 467.

46) H. E. Hallam, Vibrational Spectroscopy of Trapped Species, John Wiley and Sons, London,1973.

47) G. C. Pimentel, S. W. Charles, Pure and Appl. Chem., 1963, 7, 111

48) A. J. Barnes, J. Mol. Struct., 1980, 60, 343.

49) J. A. Warren, G. R. Smith, W. A. Guillory, J. Chem. Phys., 1980, 72, 4901.

50) B. R. Carr, B. M. Chadwick, C. S. Edwards, D. A. Long, G. C. Wharton, J. Mol. Struct.,1980, 62, 291.

51) M. T. Bowera, G. I. Kerley, W. H. Flygare, J. Chem. Phys., 1966, 45, 3399.

52) D. W. Robinson, J Chem. Phys., 963, 39, 3430.

53) M. T. Bowers, W. H. Flygare, J. Chem. Phys., 1966, 44, 1389.

54) F. T. Prochaska, L. Andrews, J. Chem. Phys., 1977, 67, 1139.

55) B. Mile, Angew. Chem. Int. Ed., 1968, 7, 507.

56) G. L. Pollack, Rev. Mod. Phys., 1964, 36, 748.

57) C. J. Purnell, A. J. Barnes, S. Suzuki, D. F. Ball, W. J. Orville-Thomas, Chem. Phys., 1976,12, 77.

58) B. I. Swanson, L. H. Jones, J. Chem. Phys., 1980, 73, 986.

59) D. Maillard, A. Schriver, J. P. Perchard, C. Girardet, J. chem. Phys., 1979, 71, 505.

60) D. Maillard, A. Schriver, J. P. Perchard, C. Girardet, J. chem. Phys., 1979, 71, 517.

61) L. Andrews, G. C. Pimentel, J. Chem. Phys., 1967, 47, 2905.

62) T. Welker, T. P. Martin, J. Chem. Phys., 1979, 70, 5683.

63) H. Dubost, L. Abouaf-Marguin, Chem. Phys. Lett., 1972, 17, 269.

64) L. H. Jones, B. I. Swanson, J. Chem. Phys., 1981, 74, 3216.

65) M. Dubs, H. H. Gunthard, Chem. Phys. Lett., 1979, 64, 105.

66) M. Poliakoff, J. J. turner, "Infrared laser photochemistry in matrixes" in "chemical and

biological application of lasers", Ed. C. B. Moore, Academic Press, New York, 1980.

67) K. Sundararajan, K. S. Viswanathan, J. Mol. Struct., 2006, 798, 109.

68) K. V. J. Jose, S. R. Gadre, K. Sundararajan, K. S. Viswanathan, J. Chem. Phys., 2007, 127,104501.

69)A. J. Barnes, L. Le Gall, C. Madec, J. Lauransan, J. Mol. Struct., 1977, 38, 109.

70) B. Walsh, A. J. Barnes, S. Suzuki, W. J. Orville-Thomas, J. Mol. Spectrosc., 1978, 72, 44.

71) J. Moore, C. Davis, M. Coplan, and S. Greer, Building Scientific Apparatus, Cambridge University Press, 2009.

72) www.arscryo.com/TechNotes.

73) S.Cradock, A.J.Hinchcliffe,Matrix Isolation, Cambridge University Press,1975.

74) A. D. Becke, Phys. Rev. A, 1989, 38, 3098.

75) A. D. Becke, J. Chem. Phys., 1983, 98, 5648.

76) C. Lee, N. Yang, R. G. Parr, Phys. Rev. B, 1988, 37, 785.

77) S. F. Boys, F. Bernadi, Mol. Phys., 1970, 19, 553.

78) F. Jensen, Chem. Phys. Lett., 1996, 261, 633.

79) I. Mayer, P. R. Surján, Chem. Phys. Lett., 1992, 191, 497.

80) D. W. Schwenke, D. G. Truhlar, J. Chem. Phys., 1985, 82, 2418.

81) L. Turi, J. J. Dannenberg, J. Phys. Chem., 1993, 97, 2488.

82) L. Turi, J. J. Dannenberg, J. Phys. Chem., 1995, 99, 639.

83) N-B. Wong,Y-S. Cheung,D. Y. Wu, Y. Ren, X. Wang, A. M. Tian, W-K. Li, J. Mol.Struct., 2000, 507, 153.

84) M. J. Frisch, G. W. Trucks, H. B. Schlegel, P. M. W. Gill, B. G. Johnson, M. A. Robb, J.R. Cheeseman, T. Keith, G. A. Peterson, J. A. Montgomery, K. Raghavachari, M. A. Al-laham, V. G. Zakrzewski, J. V. Ortiz, J. B. Foresman, J. Cioslowski, B. B. Stefanov, A.Nanayakkara, M. Challacombe, C. Y. Peng, P. Y. Ayala, W. Chen, M. W. Wong, J. L.Andres, E. S. Replogle, R. Gomperts, R. L. Martin, D. J. Fox, J. S. Binkley, D. J. Defrees, J. Baker, J. P. Stewart, M. Head- Gordon, C. Gonzalez, J. A. Pople, GAUSSIAN 09, Revision D.1,Gaussian Inc., Pittsburgh, PA, 1995.

85) Kersti Hermansson,J. Phys. Chem. A, 2002, 106, 4695-4702.

86) Yan Zhao, Donald G. Truhlar, Theor Chem Account,2008, 120,215–241.

87) Kevin E. Riley, Michal Pitonak, Petr Jurecka, and Pavel Hobza, Chem. Rev., 2010, 110, 5023–5063.

88) R. M. Bentwood, A. J. Barnes, W. J. Orville-Thomas, J. Mol. Spectrosc., 1980, *84*, 391.

89) W. V. Steele, R. D. Chirico, S. E. Knipmeyer, and A. Nguyen, J. Chem. Eng. Data 2002, 47, 689-699.